SYNTHESIS AND CHARACTERIZATION OF SILICA/SILVER MULTILAYER NANOPARTICLES AND THEIR APPLICATION IN SURFACE ENHANCED SPECTROSCOPY

A thesis presented to the faculty of the Graduate School of Western Carolina University in partial fulfillment of the requirements for the degree of Master of Science in Chemistry

By

Emily Rebecca Butcher

Director: Dr. David D. Evanoff, Jr.
Associate Professor of Chemistry
Department of Chemistry & Physics

Committee Members: Dr. Carmen L. Huffman, Chemistry
Dr. Channa R. De Silva, Chemistry

April 2015

ACKNOWLEDGEMENTS

I would foremost like to thank my research adviser Dr. David Evanoff for his constant encouragement and mentoring throughout my time at Western Carolina University. His research lab provided an engaging and academically stimulating environment for me to polish my chemistry skills and learn new skills. He has taught me real applications of the material I have learned in classes. I have been very fortunate for the opportunity to work with someone with such scientific experience and knowledge.

I'd like to thank my committee members, Dr. Huffman and Dr. De Silva, for all of their constructive feedback as I worked through the lengthy research process. Their insight throughout my project was welcome and helpful.

I'd like to thank Wes Bintz for his help with finding materials and ordering anything needed throughout my research project. His careful organization of the chemical stockroom made finding equipment simple so that my research could run as smoothly as possible. Lynley Hardie has also been a lifesaver while completing my degree, from printing flyers to helping me register for conferences.

Finally, I would like to extend my gratitude to all my family and friends for their support throughout my time at Western. I would especially like to thank my parents for being a friendly face in the chemistry department everyday, and for giving me a place to live while I completed my degree. I would also like to thank James Cook who paved the way for my research, and was always willing to help before and after he graduated. I would also like to thank the other graduate and undergraduate students I have had the opportunity to work with while at Western.

TABLE OF CONTENTS

LIST OF TABLES

LIST OF FIGURES

LIST OF ABBREVIATIONS

PVP……...polyvinyl pyrrolidone

APTMS…….(3-aminopropyl)trimethoxysilane

TEOS……tetraethyl orthosilicate

TMOS……...tetramethyl orthosilicate

$[Ru(bpy)_3]^{2+}$…….tris(2,2'-bipyridyl) dichlororuthenium (II)

RRS……...resonance Raman spectroscopy

SEM……..scanning electron microscopy

SERS…….surface enhanced Raman scattering

CSS……core/spacer/shell

ITO……indium tin oxide

TEM……..transmission electron microscopy

SEM……..scanning electron microscopy

AES……...absorption, extinction, scattering

CCD……...charge-coupled device

Abs…….absorption

ICP-OES……inductively coupled plasma emission spectrometer

NP……..nanoparticle

CV…….crystal violet

ABSTRACT

SYNTHESIS AND CHARACTERIZATION OF SILICA/SILVER MULTILAYER NANOPARTICLES AND THEIR APPLICATION IN SURFACE ENHANCED SPECTROSCOPY

Emily Rebecca Butcher, M.S. in Chemistry

Western Carolina University (April 2015)

Director: David D. Evanoff, Jr., Ph.D.

This research is focused on determining the most effective silver shell growth method for multilayered metallic nanoparticles, and determining the plausibility of using embedded $[Ru(bpy)_3]^{2+}$ as an internal standard for surface enhanced Raman spectroscopy. In the surface study, silica particles were functionalized with (3-aminopropyl)trimethoxysilane followed by a variety of seeding techniques to complete the silver shell. This study revealed that the optimum synthesis method prior to the hydrogen reduction of the silver shell utilized a tin treatment followed by a silver (I) oxide soak, resulting in the best surface coverage. Likewise extinction analysis revealed that this type of particle absorbs the most light, which likely is important for surface enhanced spectroscopy.

In the second part of the study, a procedure is reported for the synthesis of multilayered metallic nanoparticles with a dye molecule ($[Ru(bpy)_3]^{2+}$) embedded in the dielectric layer separating the two silver layers. Raman spectroscopy was used to prove the success of embedding the dye molecule into the spacer layer. Fluorescence, extinction, absorption, and scattering data were used to determine that, as the shell is synthesized, it begins to absorb more of the excitation light. This absorption is a problem because $[Ru(bpy)_3]^{2+}$ has a low quantum yield of only 7.2% and the signal is easily extinguished as the shell becomes thicker. Finally, the

particles with the embedded dye molecule were used for a preliminary test to determine their usefulness as an internal standard for surface enhanced Raman scattering. This preliminary study revealed that it is possible to detect $[Ru(bpy)_3]^{2+}$ using the 457.9 nm laser and use a 632.8 nm laser line to detect a 500 nM crystal violet solution. 500 nM is below the detection of crystal violet only using Raman spectroscopy.

CHAPTER 1. BACKGROUND

1.1 INTRODUCTION TO SILVER PLASMON RESONANCE

A plasmon resonance occurs due to the collective oscillations of conduction electrons in a metallic substance, and with at least one dimension confined to the nanometer range, such as in the case of nanoparticles. The most commonly used metallic substances with plasmons are silver, gold, and copper because their plasmons are in the visible part of the spectrum. Silver has many distinct advantages over copper and gold. For example, the plasmon of silver is well within the visible spectrum and ranges from 380 nm to 1200 nm. A second advantage of silver is that the interband transition of silver is in the UV region, so it doesn't interfere with the surface plasmon. Copper and gold both have interband transitions in the visible region. This transition is responsible for the "copper" and "gold" color that are associated with these metals. Having an interband transition in the visible region makes the plasmon of these metals less efficient than silver.[1,2] The largest disadvantage of silver is that it is toxic to biological organisms, unlike gold, which is biologically inert. This disadvantage can be overcome by coating the silver with a biologically compatible coating[3], an example of which is polyvinyl pyrrolidone (PVP). A study completed by Tejamaya et al. showed that silver particles with a PVP coating are more stable than citrate or polyethylene glycol coated silver particles. Over the course of 21 days the PVP coated particles experienced little concentration loss and no shape, aggregation, or dissolution changes in standard Organization for Economic Co-operation and Development media for *Daphnia magna*.[4]

When radiation interacts with a metallic nanoparticle or a rough metallic surface, the conduction electrons donated by the lattice atoms are accelerated in the opposite direction of the radiation's electric field. When the frequency of the incident light is at the correct frequency this

acceleration can result in the oscillation of electrons. To illustrate, consider an incident electromagnetic wave on a particle with the electric field of the wave initially pointed toward the top of the page as shown in Figure 1A. As the radiation impinges on the nanoparticle surface, the conduction electrons in the silver particles are accelerated towards the bottom of the particle resulting in a positive charge build-up at the top of the particle and a negative charge build up at the bottom (Figure 1B). This attractive force from the particle lattice begins to decelerate the electrons and this is called the restoring force. At a specific incident radiation frequency, or resonant frequency, the electric field of the radiation will switch directions (Figure 1C) as the restoring force has had maximum effect on the electrons. The result is the electrons are accelerated toward the bottom of the particle. The interplay of the oscillating electric field and the restoring force allow the particle's conduction electrons to oscillate in resonance with the electric field.[3]

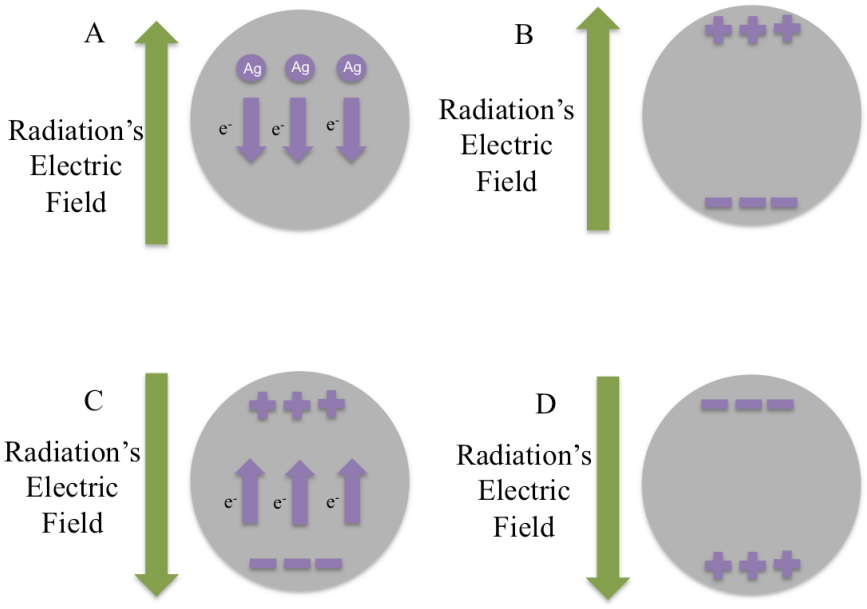

Figure 1. Electron oscillations within a metallic nanoparticle. (A) Incident radiation's electric field causes the conduction electrons in the silver atoms (purple) to accelerate towards the bottom of the particle. (B) A charge build up occurs because there is a higher electron density at the bottom of the particle. (C) The incident radiation's electric field changes direction and the positive charge build up attracts the electrons back toward the top of the particle. (D) Electrons build up at the opposite end of the particle.

In the above example it is assumed that the electric field of the incident radiation is homogeneous across the particle surface leading to the simplest oscillation, the dipole resonance, in which all conduction electrons move in unison. As the silver particle size increases however, the particle begins to experience a heterogeneous electric field from the incident radiation with respect to both magnitude and direction, causing electrons to oscillate in multiple directions simultaneously (Figure 2), resulting in multipole resonances (quadrupole, octupole, etc.).

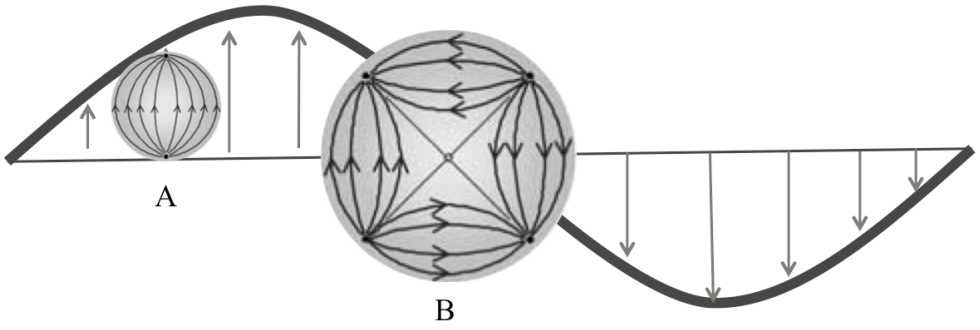

6

Figure 2. The arrows represent the direction of the incident radiation's electric field. A small silver particle (A) experiences a homogeneous electric field from the incident radiation because the particle experiences a homogenous electric field from the incident radiation. A larger silver particle (B) that experiences a heterogeneous electric field from the incident radiation results in electron oscillations in multiple directions, or a quadrupole.[3]

The restoring force determines the frequency of the electron oscillations. A higher restoring force means that there is a stronger attractive force from the positive pole of the particle, resulting in the electrons accelerating back to the positive pole more quickly. The higher the restoring force is, the higher the oscillation frequency of the electrons. The restoring force, and in consequence the oscillation frequency of the electrons, can be tuned by changing the solvent in which the nanoparticles are dispersed. If the particles are placed into a polarizable solvent, the restoring force decreases because the solvent alleviates some of the positive and negative charge build up within the particle. This results in the conduction electrons not

returning to their original position as quickly, slowing down the electron oscillations, and in turn decreasing the frequency. Polarizability is related to a solvent's refractive index. Thus, a plasmon resonance can be shifted to a longer wavelength by suspending the particles in a higher refractive index solvent.[3]

1.2 NANOPARTICLE SYNTHESIS

1.2.1 STÖBER METHOD

The classic synthesis of silica nanoparticles utilizes the Stöber method, which was first published in 1968 by Werner Stöber.[5] This reaction is either base or acid catalyzed and there are two important steps that take place: hydrolysis and condensation. As the name suggests, in hydrolysis the silicon alkoxide's alkoxy groups are replaced by hydroxyls. In the condensation step, the silanol groups begin to cross link and form particles or shells. (Figure 3)

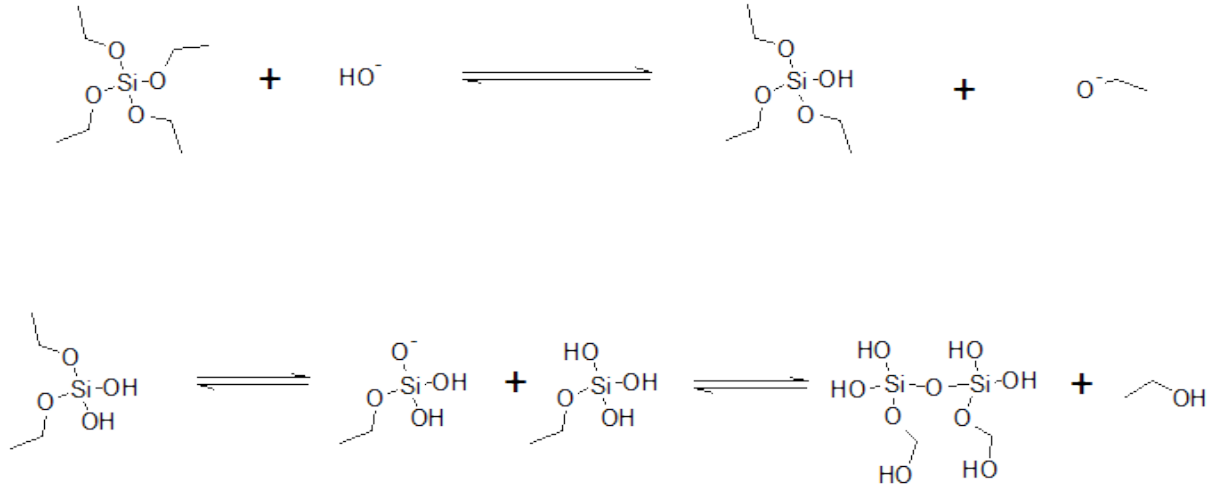

Figure 3. Stöber method: (A) Hydrolysis (B) Condensation.

Water is the donor of the hydroxyls that replace the alkoxy groups, but the silicon alkoxide molecules are hydrophobic and won't dissolve in water. In order to make the substances miscible, a co-solvent is necessary and generally an alcohol is chosen. The ratio of

water:silicon hydroxide:alcohol has a large effect on the rate and success of the hydrolysis and condensation reactions. Failure to maintain this ratio during synthesis results in the silica precursor becoming immiscible and the hydrolysis/condensation reactions will halt.[6]

1.2.2 SILVER NANOPARTICLE SYNTHESIS VIA THE CREIGHTON METHOD

A traditional silver nanoparticle synthesis method is the reduction of a silver salt by sodium borohydride and is often termed the Creighton method.[7] This synthesis method produces a concentrated solution of silver particles with a narrow size distribution of approximately 10 nm. A disadvantage of this method is the lack of control of the diameter of the silver particles produced, in other words this method is hard to adapt to synthesize particles larger than 10 nm.[3]

1.2.3 SILVER NANOPARTICLE SYNTHESIS VIA THE HYDROGEN REDUCTION METHOD

Evanoff and Chumanov first outlined the hydrogen reduction method in 2004, and it presents a simple synthesis of silver particles where the particle size can be easily controlled. In this synthesis water is saturated with silver (I) oxide and pressurized to 10 psi using hydrogen gas. The reaction is then heated to increase the speed of the synthesis. An initial burst of silver nanoparticles is observed, and as the reaction is allowed to continue, those initial particles grow in size. In this manner the size of the particles can be controlled by the length of time the suspension is under a H_2 atmosphere. The simplicity of the reaction is summarized in the overall chemical reaction (Equation 1).

$$Ag_2O(aq) + H_2(g) \rightarrow 2Ag^0(s) + H_2O(l) \quad (1)$$

This silver particle synthesis is unique because of the production of bare silver particles with only silver (I) oxide protecting the surface of the particles. The largest disadvantage with this

synthesis is that silver rods are also produced during the reduction, and a series of lengthy filtrations are required to remove the large unwanted species.[8]

1.2.4 SILICA/SILVER CORE/SHELL SEEDING AND SHELL GROWTH

Previous studies have looked at the synthesis of silica/silver core/shell particles using a modified Stöber technique. A common method to put metal nanoshells on silica cores is to first functionalize the silica surface. This process puts a functional group onto the surface of the nanoparticle, which can then act as an anchor for the seeding of a metallic nanoshell.[9] Seeding is considered necessary to ensure that, as metal atoms are reduced in the growth step, they will coalesce on the previously "seeded" particles rather than nucleating new particles in suspension. The functional groups are added to the surface of the particle through the cross-linking process previously mentioned in the Stöber synthesis. (Section 1.2.1) The cross-linking process is generally base catalyzed and requires a specific water:alcohol:precursor ratio to occur.[6] A common material used for functionalizing silica nanoparticles is (3-aminopropyl)trimethoxysilane, or APTMS. This amine functionalization attracts small nanoparticles used as seeds because the nanoparticles have a high surface curvature. The high surface curvature of the particles results in an electron deficiency at the nanoparticle surface that can be filled by the lone pair of electrons on the amine.[10–14] In a paper presented by Jackson and Halas,[11] silica nanoparticles were functionalized with APTMS and seeded with gold nanoparticles. The seeding was followed by the reduction of silver nitrate onto the surface of the nanoparticles. This method produced particles with a smooth outer shell that follows the Mie scattering theory.[11] There are a variety of similar compounds used for the functionalization of the silica surface including 3-mercaptopropyltrimethoxy-silane, vinyltriethoxysilane, 3-

aminopropyltri-ethoxysilane, and propyltrimethoxysilane.[9,15] Each of these functionalization precursors are also cross-linked onto the surface of the particle through a base catalyzed reaction.

Another proposed seeding technique involves the treatment of the silica surface with Sn^{2+}(aq) that then reduces silver onto the particle surface, and the silver then acts as a seed for the shell growth. In this technique the silica particles are synthesized using a modified Stöber method and then added to a dilute solution of HCl and tin (II) chloride. The Sn^{2+} adsorbs onto the surface of the silica, and then the particles are placed into a solution of silver nitrate. The adsorbed Sn^{2+} is then reduced to Sn^{4+} while oxidizing the Ag^{+}(aq) to Ag^{0}. The silver shell is then grown by the reduction of silver nitrate.[16] This seeding technique has been modified in our lab by using silver (I) oxide instead of silver nitrate to add silver seeds onto the silica particle surface, and then growing the silver shell using a modified hydrogen reduction technique.[17] Silver (I) oxide is advantageous over silver nitrate because it is significantly cheaper.

1.2.5 SILVER/SILICA CORE/SHELL SYNTHESIS

Multiple procedures of the synthesis of silver/silica core/shell particles have been determined.[1,18,19] These procedures are distinctly different from the synthesis of silica/silver core/shell particles because the silver does not require any surface modifications before addition of the silica shell. In one method, the silver particles are synthesized through the reduction of silver perchlorate using sodium borohydride. After synthesis of the silver particles, a solution of tetraethyl orthosilicate (TEOS) and an aqueous amine were added to the silver particle suspension. The amine catalyzed the synthesis of the silica shell. The disadvantage of this synthesis method is that the silver particle synthesis only results in one size particle diameter, and it isn't straight-forward to vary the procedure to synthesize larger particles. However, the

researchers were able to vary silica shell thickness by changing the TEOS concentration: the higher the concentration of TEOS the thicker the shell.[1]

In a second study also synthesizing silver/silica core/shell particles, the silver particles were synthesized using a hydrogen reduction method. (Section 1.2.3) The silver particles were then placed in a pyrex vessel with 2-propanol and a small amount of water. The silica shells were then synthesized by adding 600 μL of ammonium hydroxide followed by 2-60 μL of tetramethyl orthosilicate (TMOS). Again, in this reaction the shell thickness was varied by changing the concentration of silica precursor (TMOS).[19]

1.3 DYE-LABELED NANOPARTICLES USING $[Ru(bpy)_3]^{2+}$

There has been previous research exploring the addition of tris(2,2'-bipyridyl) dichlororuthenium (II), or $[Ru(bpy)_3]^{2+}$, to silicon dioxide nanoparticles but to our knowledge no research has been done creating multilayer particles with $[Ru(bpy)_3]^{2+}$ in the dielectric layer. In a study completed by Zhang, et al.[20], $[Ru(bpy)_3]^{2+}$ was embedded into silica nanoparticles and the particles were coated with a layer of silver. This research revealed a coupling between the $[Ru(bpy)_3]^{2+}$ and the metal nanoshell in the form of a more intense and more narrow emission band by $[Ru(bpy)_3]^{2+}$.[20] In a similar study, results showed that there is an optimum shell thickness for these types of particles. If the shell is too small there is no coupling and the $[Ru(bpy)_3]^{2+}$ signal isn't amplified. On the other hand, if the shell becomes too thick the signal from the $[Ru(bpy)_3]^{2+}$ is lost. There are two possibilities for the decreased signal: (1) the electromagnetic field of the shell is altered as the shell becomes thicker and dampens the signal, and (2) as the shell becomes thicker, the penetration of the $[Ru(bpy)_3]^{2+}$ emission decreases.[21,22]

1.4 RAMAN SPECTROSCOPY

When radiation interacts with matter many processes can take place, including absorption and scattering. In absorption, energy is transferred from the source radiation to the sample. In order for absorption to occur, the energy of the radiation must be of the right quanta for a transition (electronic, vibrational, or rotational) from the ground state to an excited state to take place. On the other hand, scattering is governed by the dielectric functions of the materials at an interface and doesn't require the promotion of an electron from the ground state to an excited state.[23] Instead, the incident radiation causes a momentary promotion of an electron to a virtual state, as shown in Figure 4. The immediate relaxation of the molecule from this virtual state may or may not affect the energy of the incident photon. Scattering with the same energy as the incident radiation is called elastic scattering, or Rayleigh scattering. In contrast, inelastic scattering, or Raman scattering, occurs when the scattered radiation is at a higher or a lower frequency than the incident radiation. When the scattered radiation is higher in energy it is called anti-Stokes Raman radiation, and scattered radiation that is lower in energy is called Stokes Raman radiation.[24]

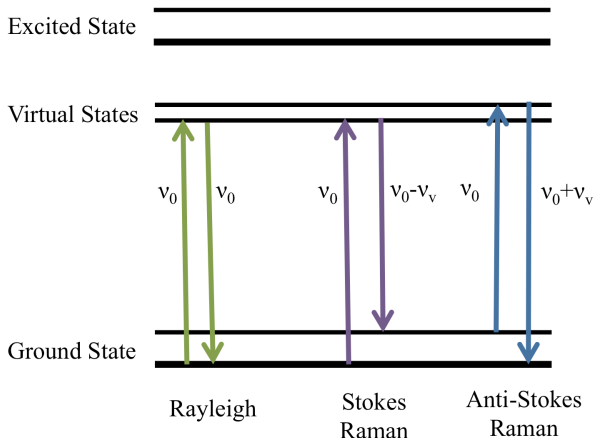

Figure 4. Diagram depicting the virtual states to which particles can be promoted and the differences in frequency for each type of scattered radiation. Here, ν_0 is the frequency of the incident radiation, and ν_v represents the difference in frequency between the incident radiation and the scattered radiation.

The inelastically scattered light is of interest in Raman spectroscopy, but a very small percentage of the scattered light is from Raman scattering. Approximately one photon out of 10^6 will be inelastically scattered; the remaining light will be Rayleigh scattered. The low probability of Raman scattering leads to a low signal during Raman spectroscopy.[24]

Whether or not a vibration is Raman active and therefore detectable by Raman spectroscopy is dependent on the polarizability of the analyte. Polarizability describes the ease to which an electric field can induce a dipole in a molecule. A vibration is only Raman active if there is a *change* in the polarizability of the molecule during the vibration. The transition moment, $[\alpha]$, for allowed transitions can be written in terms of the polarizability (α), as seen in Equation 2,

$$[\alpha] = \int \psi^*_{final}\ \alpha\psi_{initial} d\tau \qquad (2)$$

where ψ_{final} and $\psi_{initial}$ are the wavefunctions of the molecule after and before the transition respectively. The integral in Equation 2 is equal to zero unless the difference in the quantum number (v) of ψ_{final} and $\psi_{initial}$ is ± 1. Therefore, the only allowed transitions for Raman

spectroscopy are for $\Delta v = \pm 1$. If the polarizability of the sample is increased the amount of Raman scattering will increase proportionally.[25] Surface enhanced Raman scattering (SERS) techniques have been developed to increase the signal strength and decrease the detection limit of analytes by increasing the polarizability of a sample.

1.5 RESONANCE RAMAN SCATTERING

A specific type of Raman spectroscopy is resonance Raman spectroscopy (RRS). In RRS the frequency of the incident radiation overlaps or is close to the energy of the electronic transition of the analyte. The result is a coupling between the electronic transition and vibrational transitions of a molecule. When an electronic transition occurs within a molecule there can be a change in the geometry of the molecule resulting in the enhancement of the asymmetric vibrations within the excited state molecule. This coupling results in the enhancement of select normal Raman vibrational modes by a factor of 10^3-10^6. The biggest problem with RRS is that fluorescence can occur due to absorbance of the incident radiation, for analytes with an emission wavelength close to its excitation wavelength. If the analyte has a large Stokes shift, the fluorescent light will be emitted at a much longer wavelength than the incident radiation and will have little interference with the RRS signal.[26,27]

1.6 SURFACE ENHANCED RAMAN SCATTERING

The cause of surface enhanced Raman scattering (SERS) is still an active area of research, but there are two generally accepted causes of enhancement: electromagnetic and chemical. In electromagnetic enhancement, the signal intensity is increased due to the physical overlap between an analyte molecule and the electric field of a metallic plasmon, the oscillations of conduction electrons in a metallic nanoparticle. Chemical enhancement occurs because of a

charge transfer in which a bond is formed between the analyte molecule and the metallic substrate. The analyte molecule has to be in contact with the metallic substance in order for this charge transfer to occur.

1.6.1 ELECTROMAGNETIC ENHANCEMENT

Electromagentic enhancement is due to the interaction of a sample with the plasmon generated by the conduction electron oscillations in metallic nanostructures. These electron oscillations have an electric field associated with them. The electric field (E_r) extends beyond the surface of the particle as can be described by Equation 3.

$$E_r = E_o \cos\theta + g\left(\frac{a^3}{r^3}\right)E_0 \cos\theta \tag{3}$$

where E_0 is the electric field from the incident radiation, a is the radius of the particle, r is the extension of E_r from the sphere surface, θ is the angle relative to the direction of the electric field from the particle surface, and g (Equation 4) is the relationship between the dielectric constants of the metal, ε_1, and the medium, ε_0, and the frequency of the incident radiation v_L.[24,28]

$$g = \left(\frac{\varepsilon_1(v_L) - \varepsilon_0}{\varepsilon_1(v_L) + 2\varepsilon_0}\right) \tag{4}$$

If the particle is under vacuum, the dielectric constant of the medium will be exactly 1, and as a consequence, g will be maximized when the dielectric constant of the metal is -2. When the frequency of the incident radiation matches the plasmon frequency, the electric field extending out of the particle will be at a maximum, and the electric field will overlap with analyte molecules close to the metal surface. The electric field from the metallic substrate will

overlap with the analyte's electrons and increase the polarizability of the analyte. The increase in the polarizability increases the amount of Raman scattered light (cf. Equation 2). Studies have found that the most electric field enhancement occurs between two closely spaced nanoparticles. It is believed that the plasmons of the two particles overlap and couple together to form what is termed a "hot spot". If an analyte is caught in one of these hot spots, the analyte's Raman cross-section increases by 10^{12} or higher.[24,28]

1.6.2 CHEMICAL ENHANCEMENT

The second mechanism of Raman signal enhancement in SERS is due to a chemical interaction. In chemical enhancement, there is a bond between the analyte molecule and the metal surface. This bond allows for the transfer of charge from the metal's conduction band to the analyte molecule and then back to the metal. The electron transfer increases the electron density in the analyte molecule thereby increasing the polarizability of the analyte molecule and the Raman scattering signal. In order for charge transfer to occur, the analyte and the metal have to be in contact with one another as the enhancement only occurs at the surface of the metal. For example, if an analyte was deposited onto the surface of a metal in layers, only the first layer of analyte would experience charge transfer enhancement. For this reason, charge transfer is less responsible for SERS enhancement than electromagnetic enhancement.[24,26]

1.6.3 APPLICATIONS OF SERS

SERS has a wide variety of potential applications including use in cancer detection. In one study, dye-labeled gold nanoparticles were used to probe cancer cells and SERS was used to detect the nanoparticles. The probes were synthesized with a protein chain, gold nanoparticles, and a fluorescent dye. The particles were then exposed to a bioassay that simulates cancer cell

exposure and SERS was used to analyze the concentration of particles adsorbed onto the bioassay. The concentration of nanoparticles was proportional to the number of cancerous cells present in the bioassay.[29] SERS has also been explored for the detection of a variety of environmental contaminants and pathogens. The advantage of SERS is that samples can be measured quickly, and there are various handheld devices that can be implemented to take measurements in the field.[30] The addition of an internal standard would allow for the comparison between measurements taken on different days, or from different sample sites.

The reason that $[Ru(bpy)_3]^{2+}$ was chosen as the internal standard for this study is because the absorption wavelength of $[Ru(bpy)_3]^{2+}$ overlaps well with that of silver's plasmon.[2,31,32] The advantage of this overlap is that a low concentration of $[Ru(bpy)_3]^{2+}$ can be added to the particles, and a signal strong enough for Raman spectroscopy detection will be produced. Low $[Ru(bpy)_3]^{2+}$ concentrations are desirable because $[Ru(bpy)_3]^{2+}$ has fluorescent properties, and fluorescence can interfere with Raman signals.[20] $[Ru(bpy)_3]^{2+}$ also undergoes resonance Raman scattering at 457 nm, which aligns with silver's plasmon. Resonance Raman quenches the fluorescence of the $[Ru(bpy)_3]^{2+}$ significantly, further decreasing the fluorescence interference. The final advantage of $[Ru(bpy)_3]^{2+}$ is that it can be excited with the blue argon laser line (457.9 nm), and most analytes are detected using the green argon laser line (514.1 nm) or a 632.8 nm Helium-Neon laswer.[31] Thus, $[Ru(bpy)_3]^{2+}$ can be measured independently of most analytes, which eliminates concern about interference between the dye molecule and analyte signals.

CHAPTER 2. INTRODUCTION TO RESEARCH

Previous research completed in our lab by James Cook in 2014[17] revealed great promise for Ag/silica/Ag core/spacer/shell (CSS) particles but also some obvious problems. One of the biggest issues was that he couldn't measure the number of particles in his final particle suspension using the standard subtraction method because the particle shells were too fragile. In the standard subtraction method, an indium tin oxide (ITO) slide is coated with a polymer and the slide is placed into a known volume of particle suspension. The decrease in the extinction spectrum after removal of the slide is proportional to the number of particles removed from suspension. The slide can then be analyzed by electron microscopy and the number of particles on the slide surface can be counted. When the CSS particles absorbed onto the polymer substrate the outer shell was removed from the particle surface. The result was inaccurate extinction values because the shell was being removed from particles that still remained in suspension. This inspired the idea that if a more robust shell synthesis technique was established, it might be possible to count these particles using the standard subtraction method.

Cook was able to determine that SERS enhancement is possible with the CSS particles without aggregating the particles. The silver core of the CSS particles couples with the outer silver shell and creates hotspots within the particles. This eliminates the need to aggregate the particles because coupling is observed within individual particles. This led to the idea of adding a dye molecule to the spacer layer. The addition of a dye molecule would allow for the normalization of analyte signals based on the Raman signal of the dye molecule. This would ease comparison between SERS measurements.

2.1 RESEARCH OBJECTIVES

The first research objective of this study was to explore different silver shell synthesis methods and determine the different properties of these silver shells. This objective was explored using three different seeding techniques on functionalized silica particles. The possibility of synthesizing a silver shell onto functionalized silica nanoparticles without adding a metallic seed was also explored.

The second research objective of this study was to synthesize dye-labeled metallic multilayered particles. Dye-labeled silica/silver core/shell particles were synthesized using different concentrations of $[Ru(bpy)_3]^{2+}$. The final type of particle that were synthesized were dye-labeled silver/silica/silver core/spacer/shell particles. The core/spacer/shell particles were synthesized with three different outer silver shell thicknesses. These particles were explored as a possible internal standard for SERS.

2.2 SURFACE EXPERIMENTATION

The first part of this research was to determine the optimal method for the addition of a silver shell onto silica nanoparticles by altering the seeding technique being employed. In previous studies in our lab tin was adsorbed onto the surface and was used as an anchor for silver seeding.[17] In the research presented here, the particle surface was altered through the addition of an amine group onto the surface of the silica particle. The silica particles were synthesized using a modified Stöber method, followed by the addition of APTMS. The APTMS became cross-linked onto the surface of the particle by a base-catalyzed reaction. The end result was an amine group protruding off the surface of the silica particle. These amine groups act as anchors for the seeding of silver that was used to grow the silver shell. A variety of different seeding techniques

were explored including: (1) small silver particles that were synthesized using the Creighton method, (2) the reduction of silver (I) oxide by tin (II), and (3) the reduction of silver (I) oxide without tin (II). Also, growth of the silver shell without seeding was attempted. After the surface of the silver is seeded, the silver shell is grown using a modified hydrogen reduction method. In this synthesis a quartz vessel was utilized because the quartz prevents the nucleation of new silver particles. This means that new small silver particles weren't synthesized and all the reduced silver is deposited onto the surface of the silica particles.[8]

Different concentrations of APTMS were tested to determine if there was an optimal concentration of APTMS to use to functionalize the surface of the silica particles. The seeding method used to determine the optimum concentration of APTMS was seeding the silica particles with small silver particles (~17 nm) synthesized using the Creighton method. Images of the shells grown with the different concentrations of APTMS were collected using scanning electron microscopy (SEM). The particles were also analyzed using UV-visible spectroscopy to analyze the extinction spectra of each concentration.

2.3 OPTIMIZATION OF $[Ru(bpy)_3]^{2+}$ CONCENTRATIONS

Following the surface experimentation, a method was determined to add $[Ru(bpy)_3]^{2+}$ to the core of silica/silver core/shell particles. Then, different concentrations of $[Ru(bpy)_3]^{2+}$ were tested to find the optimum concentration of the dye molecule for surface enhanced Raman spectroscopy. The optimum concentration was determined using a variety of different techniques including fluorescence spectroscopy. Aliquots were collected during the growth of the silver shell, and the change in the fluorescence was determined using a fluorometer. Transmission electron microscopy (TEM) images were captured of the particles and were used to determine particle sizes and verify the successful shell synthesis.

The second part of the $[Ru(bpy)_3]^{2+}$ study was to make silver/silica/silver core/spacer/shell particles with $[Ru(bpy)_3]^{2+}$ embedded in the silica spacer layer of the particle. Various concentrations of $[Ru(bpy)_3]^{2+}$ were studied and fluorescence was also collected of the different particles. The core of the particles was synthesized using a hydrogen reduction method. The approximate size of the core was determined using UV-vis spectroscopy and confirmed with TEM images. The spacer layer was synthesized using a modified Stöber method that was base catalyzed. Finally, the silver shell was synthesized using a modified hydrogen reduction method.

CHAPTER 3. EXPERIMENTAL

3.1 MATERIALS

Research grade silver (I) oxide (99.99%) was purchased from Alfa Aesar or Strem Chemicals. Sodium borohydride, tin (II) chloride dihydrate, silver nitrate, and A.C.S. grade silver sulfate were purchased from Fisher Scientific. Tris(2,2'-bipyridyl)ruthenium (II) chloride hexahydrate (98%), anhydrous ruthenium (III) chloride (99.9%), and crystal violet were purchased from Acrōs Organics. The (3-aminopropyl)trimethoxysilane, tetraethyl orthosilicate, and tetramethyl orthosilicate were purchased from Gelest, Inc. Absolute ethanol (>99.5%), 2-propanol (>99.5%), hydrochloric acid (37.5%), ammonium hydroxide (29.5%), nitric acid (69.3%), and hydrofluoric acid (47-51%) were obtained from Fisher Scientific. All reagents were used as received and no further purification was performed.

Nylon filter membranes with a diameter of 90 mm and 0.45 μm pore size and nylon membranes with a 90 mm diameter and a 0.22 μm pore size were obtained from Fisher Scientific and VWR International. Qualitative P8 (coarse porosity and fast flow rate) filter paper with a diameter of 11.0 cm was purchased from Fisher Scientific. Ultrapure water with a resistivity of 18.2 MΩ (≤ 24 ppb TOC) was obtained from a Barnstead NANOpure Diamond system with a 0.2 μm hollow fiber filter. Copper grids (200 mesh) purchased from Electron Microscopy Sciences were used for SEM and TEM imaging.

3.2 INSTRUMENTATION

An Agilent 8453 UV-visible spectrometer was used to analyze the silver particles and the particles with silver shells. The UV-vis spectrum provided information on the size of the silver core particles, and the approximate particle concentrations. The UV-vis spectrometer also

provided preliminary evidence about the successful silver shell synthesis for the silica/silver core/shell nanoparticles and the silver/silica/silver core/spacer/shell particles. These preliminary results were then confirmed using a Hitachi 4800 scanning electron microscope (SEM), a Hitachi HD-2000 scanning transmission electron microscope, and a Hitachi HR-9500 transmission electron microscope. These electron microscopy images were also used to determine particle diameters throughout the synthesis process.

A Perkin Elmer LS-55 fluorescence spectrometer was used to collect steady state fluorescence measurements to determine the success of embedding $[Ru(bpy)_3]^{2+}$ into the silica layer of the silica/silver core/shell and the silver/silica/silver core/spacer/shell particles. The excitation wavelength used for fluorescence measurements was 450 nm and the emission spectra were collected from 500-800 nm. The excitation wavelength of 450 nm was used because $[Ru(bpy)_3]^{2+}$ has a characteristic absorption at 450 nm due to metal-to-ligand charge transfer.[20,31]

An integrating sphere was used to collect absorption, extinction, and scattering (AES) measurements of the particles synthesized. The six inch diameter, Spectralon®-coated integrating sphere was purchased from Labsphere, Inc. This integrating sphere experimental set-up utilizes the microscope and detector from a Horiba LabRam HR Raman spectrometer. The basic experimental set-up for the integrating sphere is depicted in Figure 5. The Horiba LabRam HR Raman spectrometer has a 1800 groove/mm grating, an 800 mm monochromator, and a TE-cooled charge-coupled device (CCD) detector. The systems were linked together using a 400 μm fiber optic cable and the 10x infinity-corrected plan-achromat objective (numerical aperture 0.25) of the Raman spectrometer, which was focused on the fiber optic.

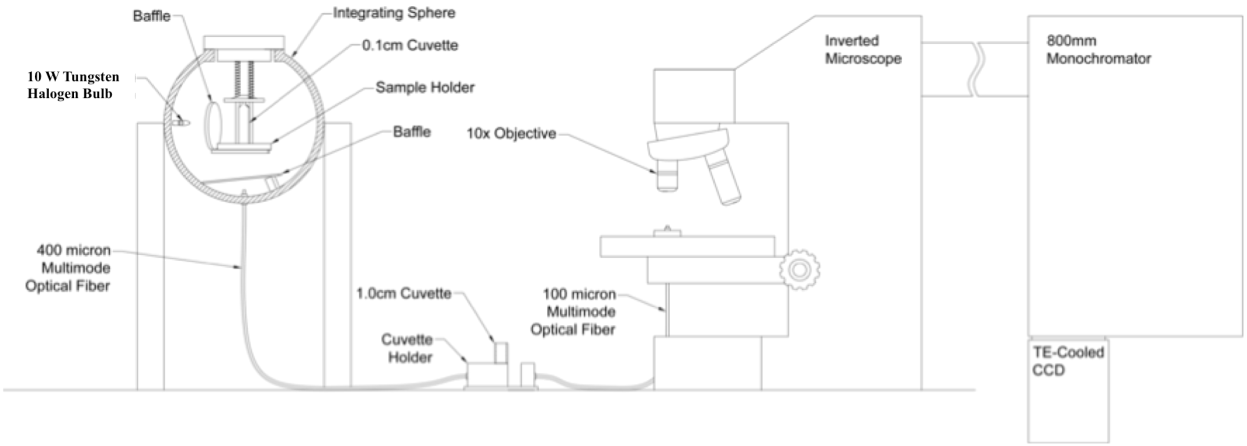

Figure 5. Instrument set-up to collect extinction, absorbance, and scattering measurements. This diagram of the instrumental set-up taken from reference 17.

A tungsten halogen bulb was used as the source in the integrating sphere. The Ocean optics CUV 1 cm cuvette holder was used to collect the extinction spectrum, which is the sum of the scattering and absorption of the particles. The absorption of the sample is then collected with the sample in the integrating sphere. The absorption (Abs) can be calculated using the following equation, where I is the intensity of the light exiting the sphere and I_0 is the intensity of the light entering the sphere (Equation 5).

$$\text{Abs} = -\log\left(\frac{I}{I_0}\right) \tag{5}$$

After the absorption is calculated the scattering of the sample can be determined by subtracting the absorption from the extinction value.

A Horiba LabRam HR Raman spectrometer (see previous description) was used to collect SERS spectra of the nanoparticles labeled with $[Ru(bpy)_3]^{2+}$. A Spectra Physics 2065-75 argon ion laser operating at a power of 160 mW and an emission wavelength of 457.9 nm with 10.3 mW power at the sample was used to collect the $[Ru(bpy)_3]^{2+}$ spectra in the particle samples. Before samples were collected, the argon ion laser was aligned using a silicon standard. Crystal violet samples were analyzed using the 20 mW Helium-Neon laser on the

Horiba LabRam HR Raman spectrometer with 7.4 mW of power at the sample. SpectraSolve 6 software was used to smooth Raman, extinction, and fluorescence data where applicable. This smoothing did not affect the shape of any of the spectra; it merely removed unwanted noise.

Finally, a Perkin Elmer Optima 4100DV inductively coupled plasma optical emission spectrometer (ICP-OES) was used to determine silver and ruthenium concentrations in the particles. The particles were dissolved in a 10% nitric acid solution with a small amount of hydrofluoric acid. The hydrofluoric acid is necessary to dissolve the silica. The dye-labeled silica/silver core/shell particles were dissolved and analyzed for the amount of ruthenium.

All of the glass vials that were used for long-term storage of the nanoparticles were cleaned using a Harrick Plasma PDC-32G plasma cleaner. The plasma cleaner removed any contaminants from the glass. This is particularly important for silver particles or particles with silver shells synthesized using the hydrogen reduction method because there aren't any stabilizing agents on the surface, but rather particles are stabilized by the electrical double layer formed by the Ag_2O (aq) species. The lack of surface groups makes the particles prone to aggregation, especially in the presence of a contaminant.

3.3 SILICA NANOPARTICLE SYNTHESIS AND FUNCTIONALIZATION

The silica nanoparticles used throughout this study were synthesized using a modified Stöber method. In this procedure, 50 mL of absolute ethanol was placed into an acid cleaned pyrex vessel. Following the ethanol, 160 µL of tetraethyl orthosilicate was added to the pyrex vessel under vigorous stirring. Finally, 2 mL of ammonium hydroxide was added drop wise to the solution. The reaction is allowed to stir over night at room temperature and then the desired concentration of APTMS is added to the vessel. The reaction is then heated to approximately 70 °C and again allowed to stir overnight. The solution is then centrifuged at 3724 g, for

30 minutes at 5 °C. The particles are then washed three times, (1) 100 % ethanol (2) 50 % ethanol: 50 % water (3) 100 % water centrifuging at 3724 g for 30 minutes at 5 °C.

3.4 FUNCTIONALIZED SILICA SEEDING TECHNIQUES

3.4.1 CREIGHTON NANOPARTICLES

The silver Creighton particles were synthesized using a 2000 mL Erlenmeyer flask with 1200 mL of ultrapure water added to it. The Erlenmeyer flask was placed into an ice bath and the temperature was allowed to equilibrate to the temperature of the ice. 0.0184 g of silver sulfate was massed and dissolved into 10 mL of water. This solution was also placed into the ice bath to cool. Two more vials were prepared one with 0.0456 g of sodium borohydride and the second with 2 mL of water. These vials were also placed into the ice bath. After all of the solutions and the Erlenmeyer of water had equilibrated to the temperature of the ice bath the Erlenmeyer was placed onto a stir plate with vigorous stirring. The silver sulfate solution was then added to the Erlenmeyer and allowed to mix for 2 minutes. The cold water was then added to the sodium borohydride, immediately sonicated for 5 seconds, and then added to the Erlenmeyer flask. The solution was allowed to stir for approximately 5 minutes and when the solution temperature was near room temperature the hotplate was turned on. The flask was heated to almost the point of boiling and until the volume of the flask was approximately 300 mL.

Following the synthesis of the Creighton particles, the particles were used to test the successfulness of the APTMS functionalization of the silica particles. In this trial silica particles were added to a solution of Creighton particles under stirring. The shift in the silver plasmon was monitored and a shift to longer wavelengths indicated the successful functionalization of the

particles. 7 mL of water were placed in a 20 mL scintillation vial and then 1 mL of Creighton silver particles were added to the vial. The vial with the Creighton particle suspension was placed onto a stir plate under constant stirring and 100 μL of functionalized silica nanoparticles were added to the vial. The solution was measured every five minutes, over the course of 40 minutes, and the shift of the plasmon of the Creighton particles was measured using a UV-vis spectrometer.

Silica particles functionalized with five different concentrations of APTMS were synthesized (Table 1) and these particles were then seeded with the Creighton silver colloid. Briefly, 30 mL of Creighton colloid was added to a 100 mL pyrex vessel and then 4 mL of the functionalized silica particles were added to the colloid. The particles were allowed to stir overnight and the particles were centrifuged at 50 g for 18-20 hours. The particles were washed twice with water. The silica particles were re-exposed to the Creighton colloid by placing 20 mL of the Creighton colloid to a reagent jar and then adding the silica particles. The particles were allowed to stir over night centrifuged, and washed twice in the same manner as previously stated.

3.4.2 TIN TREATMENT AND SATURATED SILVER (I) OXIDE SOAK

Particles were seeded using a tin treatment followed by the soaking of the particles in a saturated silver (I) oxide solution. These silica particles were functionalized in a solution with a final concentration of 5.3×10^{-3} M APTMS. First, 335 μL of 1.2 M HCl solution was added to 30 mL of water in a 50 mL conical tube. The HCl solution was necessary to dissolve the tin (II) chloride. The necessary amount of tin (II) chloride was added to the HCl solution; the amount of tin (II) chloride depended on the total surface area of the silica particles added.[16,33] The surface area was calculated by estimating the diameter of the silica particles based off past research using the same concentration of TEOS. The amount of tin (II) chloride was then determined

using the previously determined ratio of 7×10^{-8} mol/cm^2. After the addition of the tin (II) chloride the desired amount of silica nanoparticle was added to the conical tube. Finally, the final volume of the solution was brought to 40 mL to make a 0.01 M HCl solution. The silica particles were then added to the solution. The particle suspension was then sonicated for 10 minutes and then placed onto the shaker for 1 hour. The particles were then centrifuged at 3724 g, 5 °C, for 30 minutes. The particles were then washed twice with water and suspended in 5 mL of water.

After the particles were tin treated they were placed into a saturated silver (I) oxide solution. This solution was prepared by filling a 250 mL Erlenmeyer flask with 200 mL of water. A small amount of silver (I) oxide was added to a 0.22 μm filter membrane and the membrane was folded into eighths. This filter membrane was then placed into the Erlenmeyer flask of water using a cord tie, binder clip, and rubber stopper as can be seen in Figure 6 below. A small slit was cut in one end of the zip cord and a small slit was cut into the filter membrane. A piece of the cord tie was used to hang the filter membrane from the slit made on the cord tie. The apparatus was allowed to stir gently for one hour. After one hour the silica particles treated with tin were added to the Erlenmeyer apparatus and the suspension was allowed to stir for 24-36 hours. The particles were then centrifuged at 500 g, 5 °C, for 6 hours.

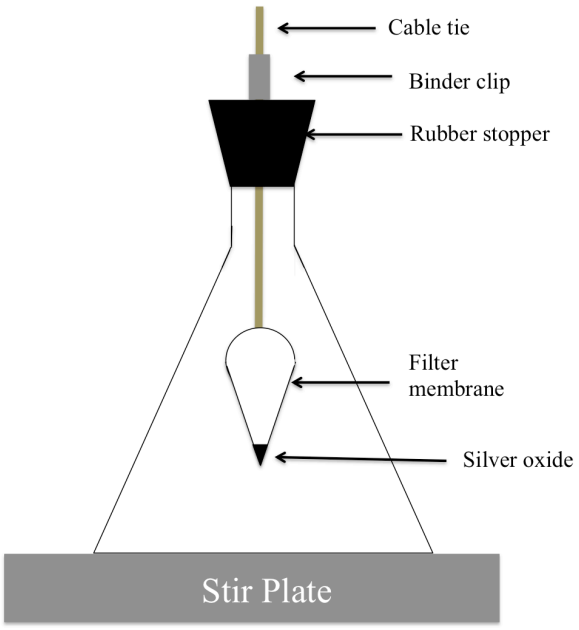

Figure 6. Filter membrane apparatus used to saturate water with silver (I) oxide before the addition of silica nanoparticles.

3.4.3 SATURATED SILVER (I) OXIDE SOAK

The saturated silver (I) oxide technique is the same as the previous seeding technique except that the surface of the silica is not treated with tin before being placed into the saturated silver (I) oxide solution. These silica particles were functionalized in a solution with a final concentration of 5.3×10^{-3} M APTMS. The water was saturated with silver (I) oxide using the same procedure previously outlined and can be seen in Figure 6. The particles were allowed to stir for 24-36 hours. The particles were then centrifuged at 500 g, 5 °C, for 6 hours.

3.4.4 SEEDLESS SHELL GROWTH

Silver shells grown on silica particles without a silver seed was also explored. These silica particles were only treated with the APTMS and then shells were grown onto the particles using

the hydrogen reduction method. These silica particles were functionalized in a solution with a final concentration of 1.1×10^{-2} M APTMS. This method was explored because, as can be seen in Section 4.1.1, while the Creighton seeds only covered a small amount of the surface of the silica particles the shells produced using the hydrogen reduction method covered the entire particles.

3.5 FUNCTIONALIZED SILICA/SILVER SHELL GROWTH

After the particles were centrifuged and concentrated, silver shells were grown using a modified hydrogen reduction method. The same shell growth method was used for each of the different seeding techniques. Briefly, approximately 0.1 g of silver (I) oxide was added to a rinsed 500 mL 3-neck quartz reaction vessel with approximately 250 mL of ultrapure water. After addition of the $Ag_2O(s)$ the vessel was placed onto a stir plate for 30-45 minutes to saturate the water with silver (I) oxide. The reaction vessel was then brought to a pressure of 10 psi using hydrogen gas and vented five times. The reduction was allowed to continue for 3 hours with 2 mL aliquots collected every 30 minutes. After three hours the reaction was bubbled with nitrogen gas for 5 minutes to remove any excess hydrogen gas and the colloid was filtered through P8 Fisherbrand Qualitative filter paper. After filtering, the colloid was centrifuged at 500 g, for 6 hours at a temperature of 4 °C.

3.6 SILICA PARTICLES EMBEDDED WITH $[Ru(bpy)_3]^{2+}$

Dye-labeled silica particles were synthesized using a modified Stöber method similar to the synthesis outlined in Section 3.3. Briefly, 50 mL of absolute ethanol was placed into a 100 mL pyrex vessel. Under stirring $[Ru(bpy)_3]^{2+}$ (aq) was added to the reaction vessel to make a final concentration of 1.96×10^{-6} M, 4.92×10^{-6} M, or 9.82×10^{-7} M. Following the addition of $[Ru(bpy)_3]^{2+}$ (aq) solution, 160 μL of TEOS was added to the reaction vessel and allowed to stir

before the addition of 2 mL of ammonium hydroxide added drop wise. The particles were then allowed to stir over night, centrifuged at 3724 g, at 5 °C, for 30 minutes. The particles were then washed 3 times with: (1) 100% ethanol, (2) 50% ethanol:50% water, and (3) 100% water using the same centrifuge settings.

3.7 SILICA/SILVER CORE/SHELL PARTICLES EMBEDDED WITH $[Ru(bpy)_3]^{2+}$

The dye-labeled silica cores are synthesized using the technique outlined in the previous section. The dye-labeled silica particles were then treated using the tin treatment and silver (I) oxide soak method outlined in Section 3.4.2. After the silver (I) oxide soak, the particles were centrifuged at 500 g, 4 °C, for 6 hours and stored in a 15 mL conical tube until the shell synthesis. After the particles were seeded, silver shells were synthesized using a modified hydrogen reduction method as outlined in Section 3.5.

3.8 SILVER CORE SYNTHESIS-CSS PARTICLES

Silver nanoparticles, which were used as core in CSS particles, were synthesized using the hydrogen reduction method as outlined by Evanoff and Chumanov[8]. Briefly, 3 grams of silver (I) oxide and 4000 mL of ultra pure water are placed into a 5000 mL 3-neck pyrex vessel. This vessel is then heated to 70 °C, and after the temperature has equilibrated, the vessel is placed under a pressure of 10 psi using hydrogen gas. This method is a time dependent reaction and the longer the reaction is allowed to run (the longer the vessel is pressurized), the larger the silver nanoparticle diameter. After the suspension has cooled, it is filtered twice, through a 0.45 μm and a 0.22 μm nylon filter membrane. The silver colloid is then centrifuged at 150 g, 4 °C, for 8 hours and then stored in a plasma cleaned glass vial.[8,34]

3.9 DIELECTRIC LAYER WITH EMBEDDED $[Ru(bpy)_3]^{2+}$ SYNTHESIS-CSS PARTICLES

The dielectric layer of CSS particles was synthesized using a modified Stöber method. All of the reagents and vessels used for this synthesis were placed into a cold room (4 °C) at least 12 hours prior to the synthesis. The entire synthesis was also performed inside a cold room. In this synthesis a silver nanoparticle suspension is combined with ultrapure water that has been saturated with silver (I) oxide. The surface area of the particles determines the amount of particle suspension and saturated silver (I) oxide water that are used during the synthesis. The total surface area of the silver particles was kept to 1.30×10^{17} nm^2. The approximate silver nanoparticle diameter was determined based on the, plasmon, position in the UV-vis spectrum. The approximate particle concentration is then calculated based on the extinction of the silver nanoparticles. The amount of silver colloid necessary to achieve this total surface area is calculated and the amount of saturated silver (I) oxide is calculated by subtracting the amount of silver colloid from 8 mL (the total suspension volume should be 8 mL). The saturated silver (I) oxide solution is then added to a 20 mL scintillation vial and the silver colloid is added drop wise to the vial. The next step is to place 50 mL of 2-propanol into a 100 mL pyrex vessel. Under constant stirring the nanoparticle and water suspension is added drop wise to the pyrex vessel. The solution is allowed to stir at least 10 minutes to ensure that the silver particles do not aggregate. After the ten minutes have passed, 600 μL of ammonium hydroxide, then 30 μL of tetramethoxysilane, and finally the desired amount of $[Ru(bpy)_3]^{2+}(aq)$ are added rapidly to the vessel, in the presented order. Varying the amount of TMOS will change the thickness of the silica shell.[35]

3.10 SEEDING SILVER/SILICA-CSS PARTICLES

The seeding technique employed for the shell growth was adapted from the tin treatment and the silver (I) oxide soak previously outlined in the surface study. The first step was to determine the approximate surface area of the silver/silica core/shell particles. The surface area was determined by approximating the diameter of the silver shell using the plasmon position on the UV-vis spectrum, and then estimating the silica shell thickness based off previous research. The diameter was then used to calculate the surface area of each particle. The particle concentration was then determined based off the UV-vis extinction spectrum of the silver cores. It was previously determined that the ratio of tin (II) chloride to silica surface was 7×10^{-8} mol/cm^2. This ratio was used to determine the amount of tin (II) chloride to add to the reaction vessel.

After the desired amount of tin was determined, 30 mL of ultrapure water was placed into a conical tube. Then 335 μL of 1.2 M HCl was added to the conical tube to help dissolve the tin (II) chloride. The HCl was followed by the calculated amount of $SnCl_2$, and finally the dye-labeled silver/silica core/shell nanoparticle suspension. The final volume was then brought to 40 mL to make a 0.01 M HCl solution. The particle suspension was then sonicated for 10 minutes and placed onto the shaker for 1 hour. Finally, the particles were centrifuged at 500 g, 4 °C, for 5 hours and dispersed in water. This centrifuge procedure was repeated twice to wash the particles in water.

After the surface of the particles was treated with tin, the particles were placed into a 250 mL Erlenmeyer flask with water that was saturated with silver (I) oxide. The water was saturated with silver (I) oxide using the same procedure outlined in the particle surface study (Section 3.4.2). The soaking apparatus is summarized in Figure 6. The tin-treated particles were

added to the saturated silver (I) oxide water solution and allowed to stir for 24-48 hours. The particles were then centrifuged at 500 g, 4 °C, for 6 hours. The excess water was removed after centrifuging and the particles were placed into a 15 mL conical tube until the shells synthesis.

3.11 SILVER SHELL SYNTHESIS-CSS PARTICLES

The silver shell of the silver/silica/silver core/spacer/shell particles was synthesized using a modified hydrogen reduction technique as outlined in Section 3.5. Briefly, approximately 0.1 g of silver (I) oxide was added to a quartz vessel and the vessel was pressurized to 10 psi with hydrogen gas. This was followed by the desired amount of the seeded silver/silica particles. A preliminary reaction was run for three hours and aliquots were collected every 30 minutes and analyzed in the fluorometer and integrating sphere to determine an ideal reaction time. These revealed that after 3 hours the $[Ru(bpy)_3]^{2+}$ signal is undetected with Raman spectroscopy.

A second preliminary study was completed where a two and half-hour reaction was ran and aliquots were collected every five minutes. These aliquots were then analyzed with Raman spectroscopy to determine the time at which the $[Ru(bpy)_3]^{2+}$ signal became undetectable. These aliquots were also analyzed with the UV-vis spectrometer and the fluorometer. After this study was completed, the same reaction was completed twice more with a 30 minute reaction time and a 90 minute reaction time.

CHAPTER 4. RESULTS AND DISCUSSION

4.1 SURFACE STUDY RESULTS

4.1.1 CREIGHTON PARTICLE RESULTS

The success of the addition of APTMS to the surface of the silica particles was determined by exposing a small amount of the silica particles to Creighton particles, and a shift in the silver particle plasmon was observed. As can be seen in Figure 7, the Creighton plasmon shifts to longer wavelengths. This shift occurs because the silver particles are in close proximity to the silica. Silica has a higher refractive index than the water in which the particles are suspended. The higher refractive index of silica causes the electron oscillations in the silver particle to slow down because of a reduced restoring force, and the plasmon shifts to longer wavelengths. The likelihood of this shift happening by chance is very low because the silica particle concentration is low.

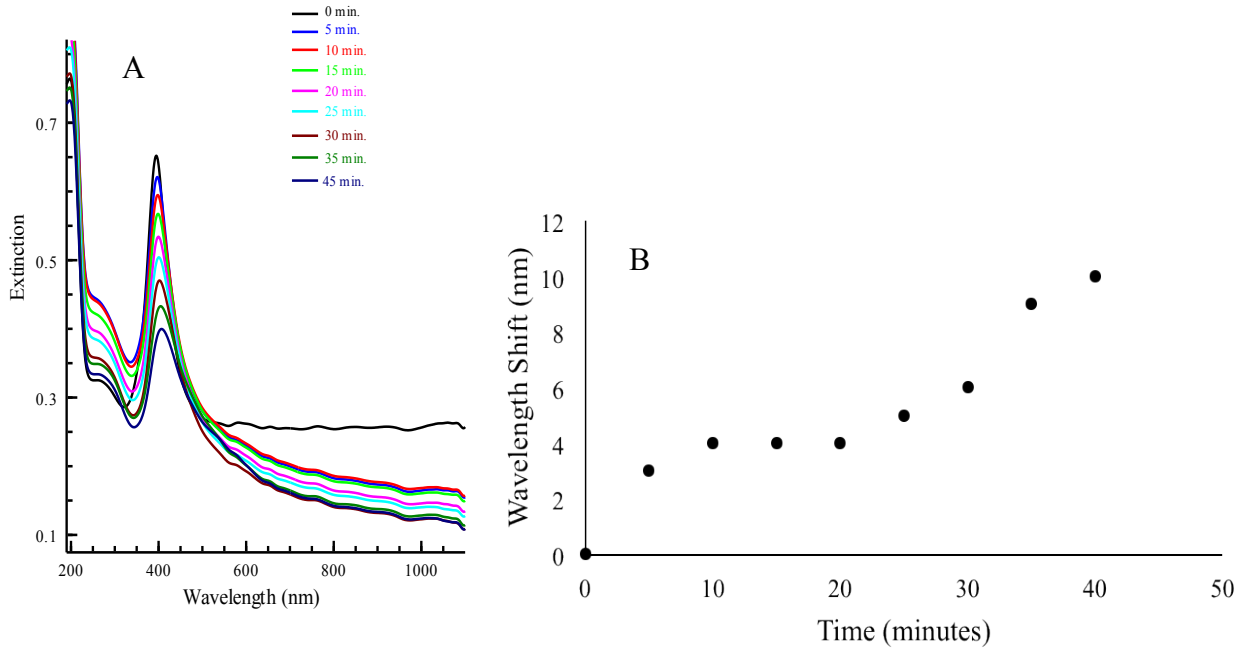

Figure 7. (A) UV-vis spectra of Creighton particle adsorption on to functionalized silica particles. The suspension was measured every 5 minutes and the plasmon maximum was seen to shift from 394 nm to 404 nm (B).

After confirming the success of the functionalization process, silica particles were synthesized using five different concentrations of APTMS. The concentrations of APTMS are summarized in Table 1 along with the particle diameters. The silica/silver core/shell diameters are approximate due to a limited number of available particles for measurement. Also, the diameters of the core/shell particles are in general smaller than the diameters of the bare silica particles. It is possible that the silica layers are collapsing or dissolving during shell growth. This is addressed further in Section 4.3.1.

Table 1. Summary of APTMS concentrations, nanoparticle diameters without the shell, and nanoparticle diameters after shell growth.

Label	APTMS (M)	Bare Particle Diameter (nm)	Core/shell Diameter (nm)
A	1.1×10^{-3}	219 ± 20	190 ± 15
B	2.6×10^{-3}	196 ± 24	185 ± 14
C	5.3×10^{-3}	223 ± 10	235 ± 32
D	1.1×10^{-2}	219 ± 14	180 ± 20
E	1.6×10^{-2}	209 ± 28	180 ± 20

UV-vis spectra were also collected of the all the silica/silver core/shell particles and are presented in Figure 8. These spectra have been offset in the vertical direction to make comparison easier. The UV-vis data also support the formation of silver shells on the particles because the plasmon broadens and shifts to longer wavelength compared to the seeded particles. There isn't a trend that can be drawn when comparing the different concentrations of APTMS. It was expected that as the concentration of APTMS increases, the silver shell would become more dense resulting in a broad plasmon that ranges from approximately 350-700 nm, indicating a denser silver shell. However, it can be seen that all of the spectra have short wavelength features (~450 nm) likely attributed to single islands of silver. The only exception are the particles synthesized using 5.3×10^{-3} M APTMS solution, but this could just be by chance.

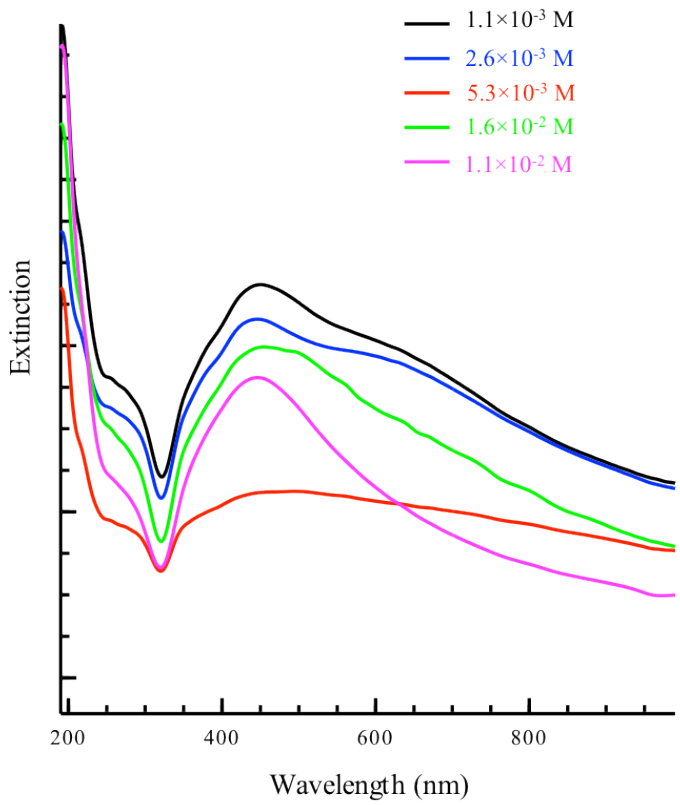

Figure 8. UV-vis spectra of silica/silver core/shell particles produced using five different concentrations of APTMS.

The plasmon broadening can be seen more clearly in Figure 9 for each of the different APTMS concentrations, which compares the Creighton, seeded particles with the silica/silver core/shell particles. The overlaid spectra reveal that the short wavelength features are at approximately the same wavelength as the Creighton seeds.

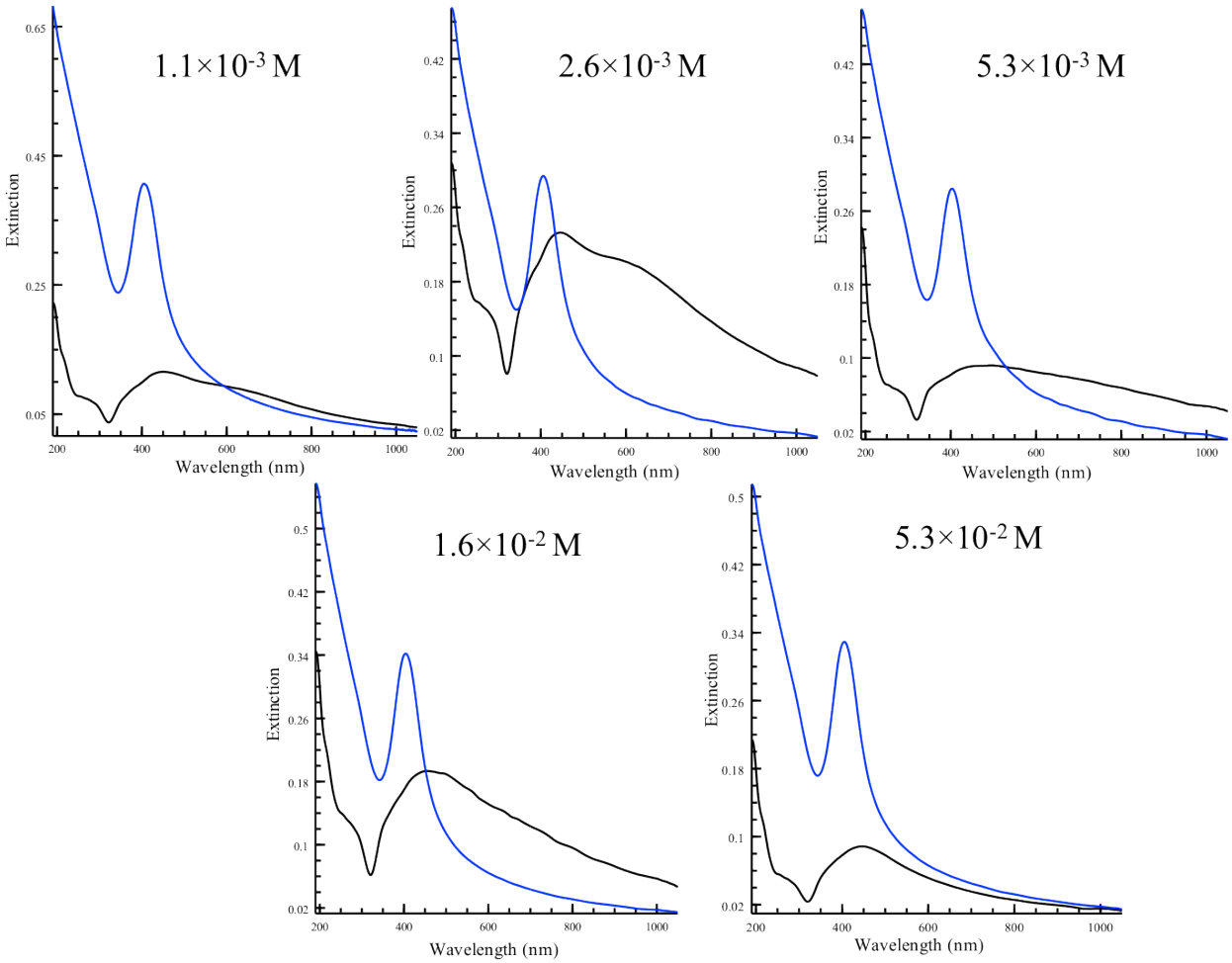

Figure 9. UV-vis spectra of functionalized silica particles seeded with Creighton silver particles (blue) and silica/silver core/shell particles (black). The letters designate different concentrations of APTMS (**Table 1**).

Representative images of the silica nanoparticles, the seeded silica particles, and the silica/silver core/shell particles are displayed in Figure 10. These images were collected of particles synthesized with the lowest concentration of APTMS, 1.1×10^{-3} M. The large masses of silver on the final silica/silver core/shell particles are from the Creighton particles used for seeding the silica particles. The Creighton particles are approximately 17 nm in size. During the hydrogen reduction synthesis more silver is deposited on top of these 17 nm size islands. The

result is that the islands of silver become much larger and these large islands are undesirable for SERS applications. These large islands of silver led to the exploration of other seeding techniques in an attempt to make smoother silver shells.

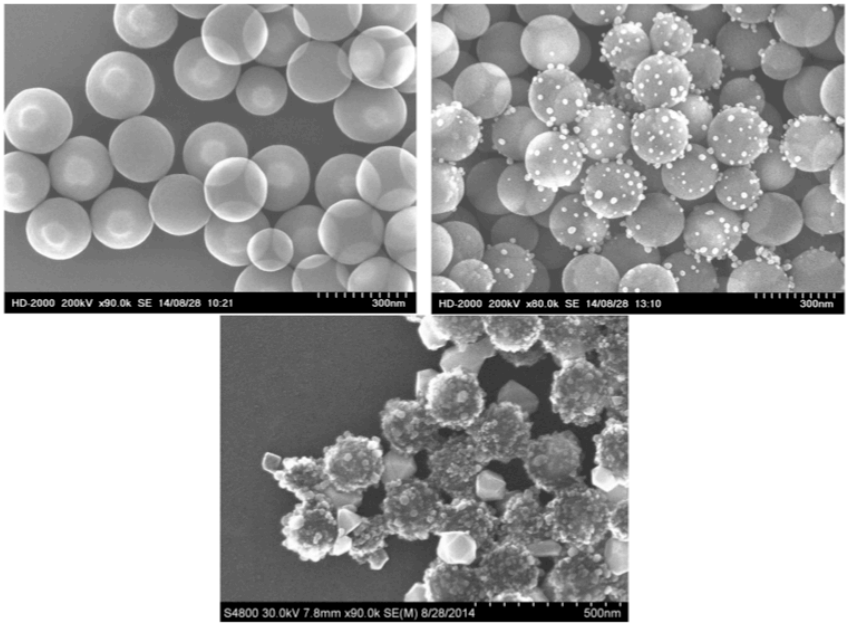

Figure 10. SEM images of silica nanoparticles functionalized with a $1.1x10^{-3}$ M concentration of APTMS (top left), silica nanoparticles seeded with Creighton colloid nanoparticles (top right), and silica/silver core/shell nanoparticles (bottom).

Figure 10 also shows that the silica particles are not evenly covered with the Creighton particle seeds. Also, some of the seeded silica particles do not have any Creighton silver particles on the surface, but all of the particles have silver shells grown on the surface. This was the logic for testing the hydrogen reduction shell growth technique without seeding the surface. These images support the hypothesis that silica particles without seeds can grow silver coatings.

4.1.2 DIFFERENT SURFACE TREATMENTS

Three different surface treatments were explored during this study including silver (I) oxide soak with tin treatment, seedless shell growth, and silver (I) oxide soak without tin treatment. It should be noted that a higher concentration of APTMS was used to functionalize the seedless

shell growth particles compared to the silver (I) oxide soak with tin treatment and the silver (I) oxide soak without tin treatment. The concentrations of 5.3×10^{-3} M and 1.1×10^{-2} M were chosen because the previous APTMS study didn't reveal any definitive difference in the success of the different APTMS concentrations. For this reason, two of the middle APTMS concentrations were chosen for the functionalization of the surface study particles.

The particles from the tin treatment followed by the silver (I) oxide soak have a broad plasmon indicative of a silver shell. The suspension color of the tin treatment and then the silver (I) oxide soak silica/silver core/shell particles looked the most similar to silica/silver core/shell particles previously synthesized in this lab using the tin treatment method without APTMS functionalization.[17] The particle suspension appeared as a dark brown color after the shell growth. The seedless shell growth particle suspension appeared as a dark gray color. It was also noted that the silver (I) oxide soaked particles without the tin treatment were difficult to centrifuge. It appears that there was some type of change to the surface of the particle making the particles more difficult to extract from suspension. These particles would have been explored further, but due to time constraints the tin treatment method was adopted for the remainder of the study. TEM images were collected of the particles and are shown in Figure 11.

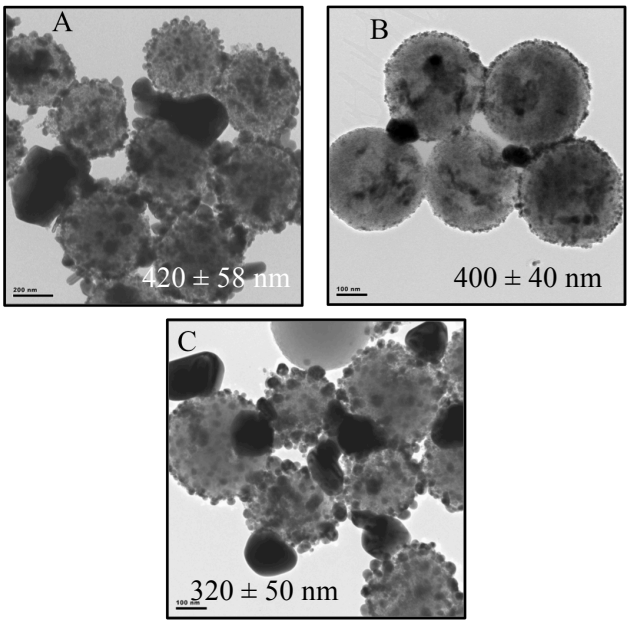

Figure 11. TEM images of the silica/silver core/shell particles synthesized with different seeding techniques. (A) Sn treatment and silver (I) oxide soak, (B) seedless shell growth, (C) silver (I) oxide soak.

It is interesting to note that all of the seeding techniques resulted in shells. The most surprising shell growth was observed when no seed was used (Figure 11B). It is generally accepted in the literature that the only way to synthesize a metallic shell is by first seeding the particle surface.[10–14] This research has shown that if the hydrogen reduction shell synthesis is used, a shell can be synthesized without any seed if the core particles are functionalized silica. The extinction spectra of all four different particle suspensions after synthesis of the silica/silver core/shell particles are displayed in Figure 12. It can be seen that all of the different treatments result in broad plasmons, which are indicative of shell formation.

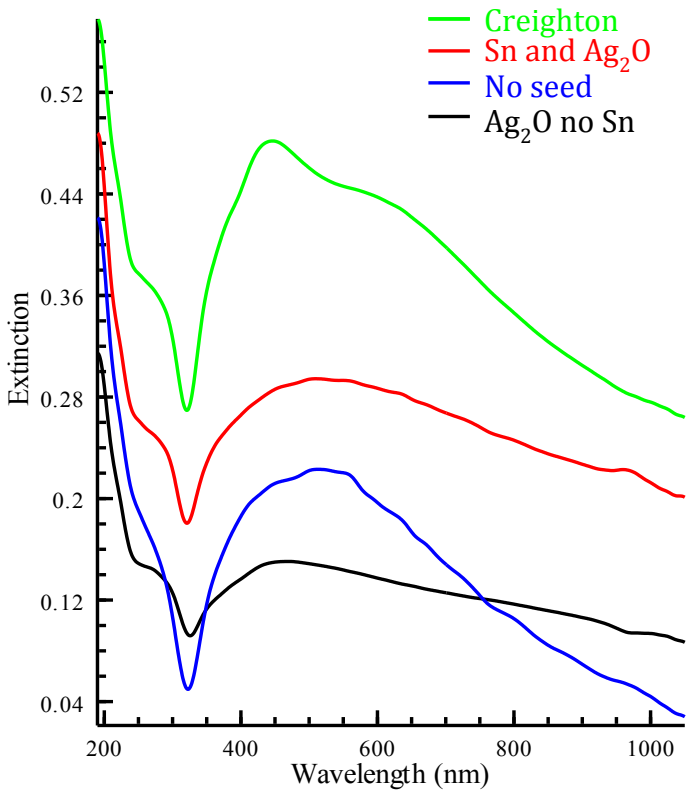

Figure 12. Extinction spectra of the plasmon of the silica/silver core/shell particles synthesized with each of the four different seeding techniques.

Absorption, extinction, and scattering measurements were also collected for each type of particle. It can be seen in Figure 13 that the functionalized particles that underwent the tin treatment followed by the silver (I) oxide soak had the highest ratio of absorption to scattering at a wavelength of 500 nm (0.55:0.3) while the particles that were only exposed to the silver (I) oxide soak had the lowest ratio (0.05:0.35). This means that the tin treatment followed by the silver (I) oxide soak resulted in the best shells for Raman applications because of the larger absorption component. When radiation interacts with a particle, the radiation causes the free electrons in the particle to oscillate (plasmon resonance). The energy of these electron oscillations is dissipated through resonant scattering and absorptive modes, the relative ratio of

the modes being governed by the complex dielectric function of the metal with respect to the plasmon frequency. Plasmon relaxation via resonant scattering results in the emission of a photon and typically occurs within 4 fs. In absorptive relaxation, the energy of the plasmon resonance is transferred into a particle phonon mode (oscillations of the lattice atoms within the particle) and thus is dissipated as heat. The absorptive relaxation mode typically begins around 40 fs after plasmon excitation, which is significantly longer than scattering. Our hypothesis is that the greater degree to which the particle plasmon resonance energy is dissipated through absorptive modes, the longer the local electric field around a particle undergoing a plasmon resonance will last. During Raman measurements, if this electric field extends off the surface of the particle for a longer period of time, the chance that an analyte will be in close proximity to the particle and experience SERS increases.

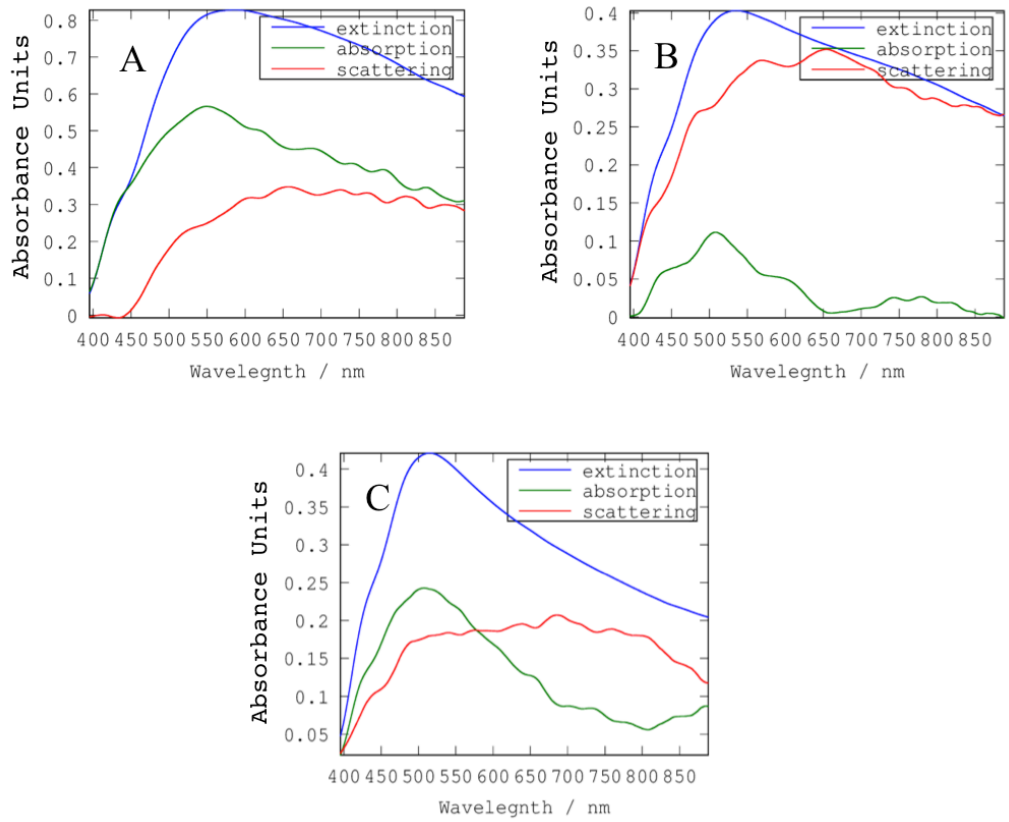

Figure 13. AES measurements of the different functionalized silica/silver core/shell particles synthesized using different seeding techniques including: (A) the tin treatment followed by the silver (I) oxide soak, (B) only the silver (I) oxide soak, and (C) seedless shell growth.

4.2 SILICA/SILVER WITH $[Ru(bpy)_3]^{2+}$ IN DIELECTRIC CORE

There were three different concentrations of $[Ru(bpy)_3]^{2+}(aq)$ used to synthesize dye-labeled silica/silver core/shell particles. The different concentrations, bare silica particle diameters, core/shell particle diameters, and the concentration of $[Ru(bpy)_3]^{2+}$ per nanoparticle are summarized in Table 2. The total particle diameter of the particles synthesized with 1.96×10^{-6} M $[Ru(bpy)_3]^{2+}$ was not included because the images were not obtained due to time constraints. The $[Ru(bpy)_3]^{2+}(aq)$ concentrations expressed in units of molarity represent the concentration of $[Ru(bpy)_3]^{2+}$ (aq) in the original reaction vessel. The concentration of

$[Ru(bpy)_3]^{2+}$(aq) per particle in the suspension was calculated based on the assumption that all of the $[Ru(bpy)_3]^{2+}$ was incorporated into the particles. This assumption was made because the supernatants collected during synthesis and during the washes of the particles didn't produce a detectable $[Ru(bpy)_3]^{2+}$ fluorometric emission spectrum.

Table 2. Concentrations of $[Ru(bpy)_3]^{2+}$(aq), core/shell particle diameters, shell thicknesses, and the concentration of $[Ru(bpy)_3]^{2+}$per nanoparticle (NP).

$[Ru(bpy)_3]^{2+}$(aq) Concentrations (M)	Bare Particle Diameter (nm)	Core/shell Particle Diameter (nm)	Concentration $[Ru(bpy)]_3^{2+}$/NP (molecules/NP)
9.82×10^{-7}	417 ± 47	361 ± 38	7.69×10^3
1.96×10^{-6}	503 ± 25	Unknown	1.07×10^4
4.92×10^{-6}	446 ± 28	467 ± 36	2.67×10^4

Following the synthesis of the dye-labeled silica/silver core/shell particles, emission intensity data of particle suspensions was collected along with $[Ru(bpy)_3]^{2+}$ (aq) in water and the spectra are provided in Figure 14. This data hasn't been normalized for the concentration of $[Ru(bpy)_3]^{2+}$ but some general trends are apparent. In all four spectra there is a peak around 600 nm, which is characteristic of $[Ru(bpy)_3]^{2+}$ and indicates that $[Ru(bpy)_3]^{2+}$ was incorporated into the nanoparticles. The emission shift to longer wavelengths and the peak broadening could be due to an interaction between $[Ru(bpy)]_3^{2+}$ and the silica.

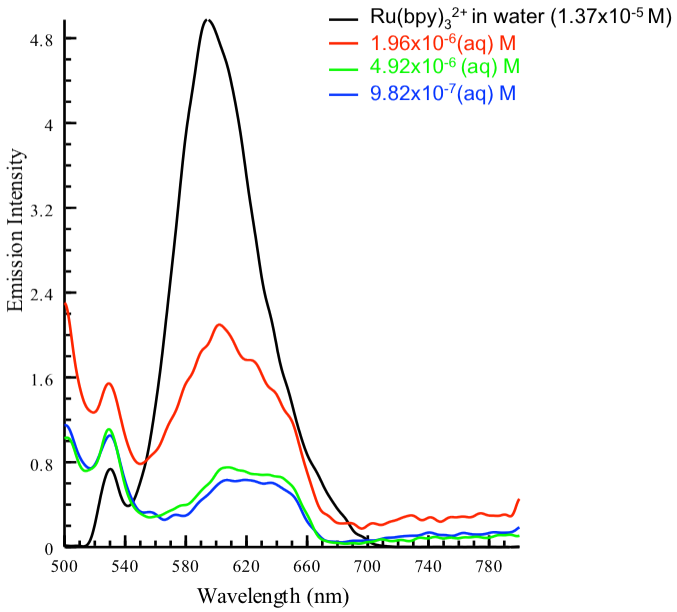

Figure 14. Emission spectra of the silica-silver core-shell particles with different concentrations of $[Ru(bpy)_3]^{2+}$in the silica core and the emission spectra of free $[Ru(bpy)_3]^{2+}$(aq).

AES spectra and TEM images were collected of each of the different particles. It can be seen that the lowest $[Ru(bpy)_3]^{2+}$concentration results in the highest absorption to scattering ratio at 550 nm (Figure 15). It can also be noted that the extinction is broadened after the dye addition and this is likely due emission from the $[Ru(bpy)_3]^{2+}$.

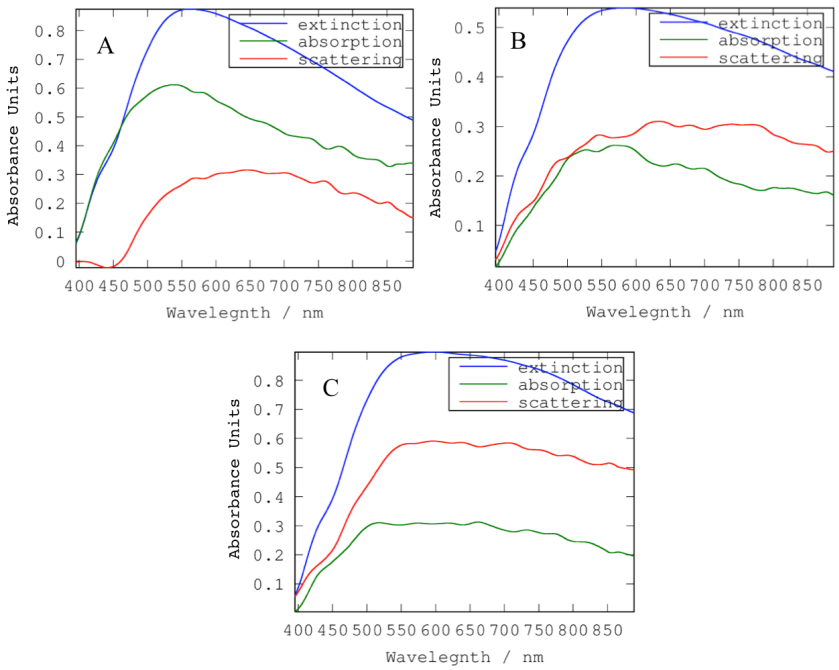

Figure 15. AES of the dye-labeled silica/silver core/shell particles (A) 9.82×10^{-7} M (B) 4.92×10^{-6} M (C) 1.96×10^{-6} M.

The TEM images (Figure 16) revealed complete particle coverage and were used to calculate the core/shell particle diameters.

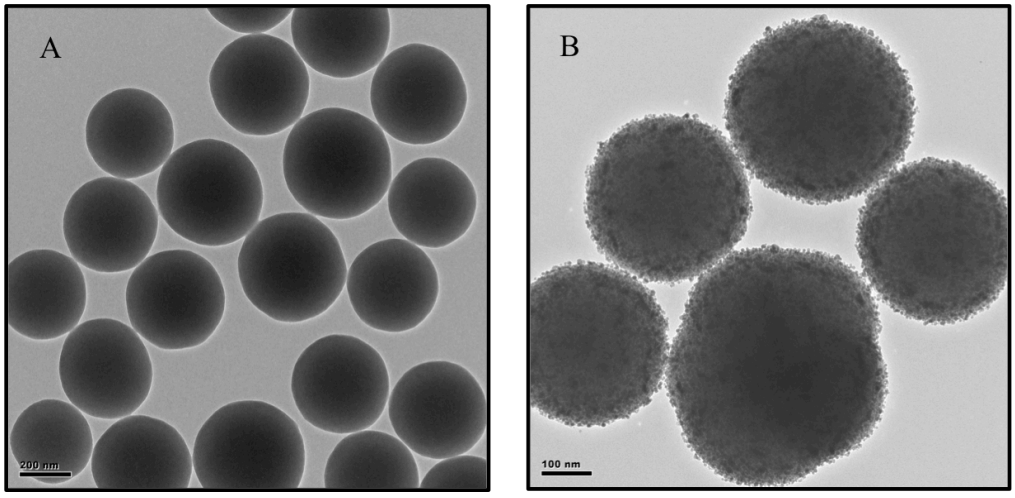

Figure 16. TEM images of the silica core particles (A) and the silica/silver core/shell particles (B) synthesized with 9.82×10^{-7} M $[Ru(bpy)_3]^{2+}$.

A brief study was also completed looking at the functionalization of the dye-labeled silica/silver core/shell particles. In this study, the previously established technique for the

synthesis of functionalized silica particles was explored. This study revealed that the silica particles were more prone to aggregation during the functionalization process after the addition of $[Ru(bpy)_3]^{2+}$ (aq). Due to time constraints, the adaptation of the functionalization procedure wasn't pursued and the previously established seeding technique using the tin treatment followed by the silver (I) oxide soak was utilized in the remainder of the study.[17]

The ICP-OES data collected during this experimentation didn't result in very conclusive data. The synthesis methods employed in this experimentation do not yield enough particles for digestion to get definitive values. However, concentration ranges were obtained for the two highest $[Ru(bpy)_3]^{2+}$ concentrations and are summarized in Table 3. The concentration of $[Ru(bpy)_3]^{2+}$/NP in units of molecules/particle in Table 3 were compared with the values summarized in Table 2, and the concentrations in Table 2 are within the concentration ranges obtained using ICP-OES.

Table 3. Ruthenium concentrations of the 1.96×10^{-6} M and 4.92×10^{-6} M dye-labeled particles as detected by ICP-OES.

$[Ru(bpy)_3]^{2+}$(aq) Concentrations (M)	Concentration $[Ru(bpy)_3]^{2+}$/NP (ppb/NP)	Concentration $[Ru(bpy)_3]^{2+}$/NP (molecules/NP)
1.96×10^{-6}	1.6×10^{-10}-7.2×10^{-10}	9,600-43,000
4.92×10^{-6}	1.1×10^{-9}-5.0×10^{-9}	6,800-300,000

4.3 SILVER/SILICA/SILVER CSS PARTICLES

4.3.1 SILVER/SILICA/SILVER CSS PARTICLES WITH A 30 MINUTE SHELL SYNTHESIS

After synthesis of the three layer particles, TEM images were collected to determine the diameters of the particles. The TEM images are presented in Figure 17.

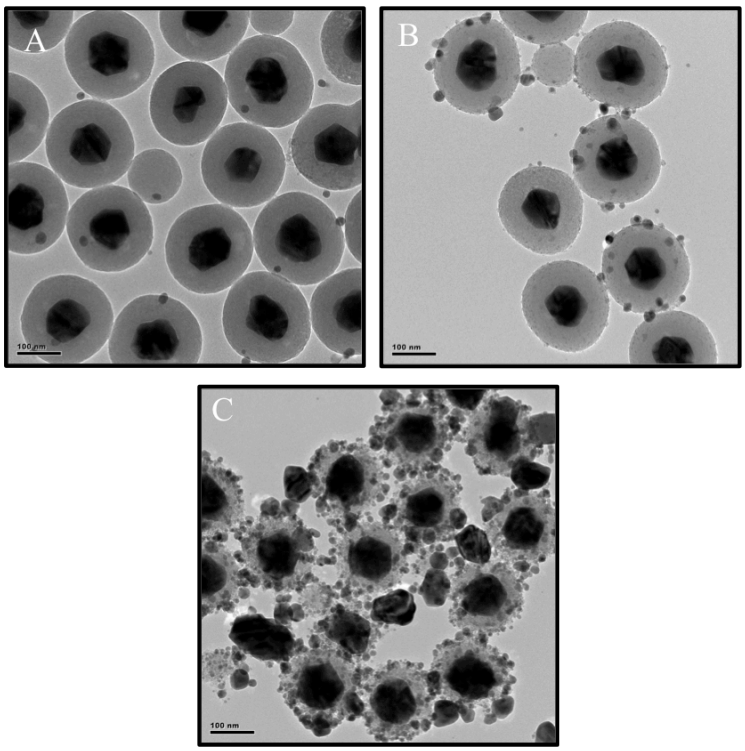

Figure 17. TEM images of the CSS particles at different stages in the synthesis process (A) after the synthesis of the silica spacer shell, (B) after the seeding of the particles, and (C) after a 30 minute shell synthesis.

The particle diameters are summarized in Table 4, and they reveal that after the addition of the outer shell the total particle diameter decreases. This could be attributed to the fact that the hydrogen reduction shell growth is done under slightly basic conditions[8] and the silica could be dissolving into solution during the reaction. Likewise, base-catalyzed silica synthesis is known to produce much more porous silica as compared to acid-catalyzed reactions.[6] It is possible that during the shell synthesis, pores in the silica spacer layer are collapsing, causing the layer thickness to shrink.

The number of molecules of $[Ru(bpy)_3]^{2+}$ per particle was calculated as 29,000. This number was calculated assuming that all of the $[Ru(bpy)_3]^{2+}$was incorporated into the silica spacer layer. This was assumed because during the synthesis of dye-labeled silica particles the supernatants were analyzed using the fluorometer, and there was no fluorescence signal from

$[Ru(bpy)_3]^{2+}$ (aq) after the reaction, indicating that most of the dye was incorporated into the particles. This is a conservative estimation because it over estimates the amount of $[Ru(bpy)_3]^{2+}$ that was incorporated into the particles.

Table 4. Summary of the core diameter, spacer thickness, CSS total diameter, and the concentration of $[Ru(bpy)_3]^{2+}$ in the CSS particles synthesized for preliminary characterization.

Core Diameter (nm)	Spacer Thickness (nm)	CSS Total Diameter (nm)	Concentration $[Ru(bpy)_3]^{2+}$/NP (molecules/NP)
92 ± 10	52 ± 4	179 ± 38	2.90×10^4

The decrease in the spacer layer during the shell synthesis was inspected more closely by measuring the spacer thickness at different times during the shell synthesis. These results are summarized in Table 5. It should be noted that seeding the particles doesn't have an effect on the spacer shell size but during the hydrogen reduction the spacer layer thickness slowly decreases with most of the loss occurring in the first 10-15 minutes. At present this decrease is being attributed to the basic conditions of the hydrogen reduction reaction.

Table 5. Spacer layer thickness throughout synthesis of CSS particles.

Synthesis Step	Spacer Thickness (nm)
Ag/silica core/shell	52 ± 4
Ag/silica & seed core/shell particles	53 ± 3
10 minutes into H_2 shell reduction	48 ± 4
15 minutes into H_2 shell reduction	42 ± 6
20 minutes into H_2 shell reduction	40 ± 4

Extinction spectra were collected using a UV-vis spectrometer of each of the different steps during the synthesis of the CSS particles with silver shells grown for 30 minutes (Figure 18). After the addition of the dye-labeled spacer layer there is a shift towards longer wavelengths. This shift is due to the silica layer on the silver core. Silica has a higher refractive index than the water in which the particles are suspended. The higher refractive index of the silica causes the frequency of electron oscillations in the silver core to decrease, which shifts the

spectral position of the plasmon resonance to longer wavelengths. The CSS also experiences a slight broadening due to the outer silver deposition. The lack of long wavelength component of the extinction spectrum, however, likely indicates that 30 minutes is not enough time for growth to allow the individual silver grains of the outer shell to cooperatively exhibit a shell plasmon resonance.

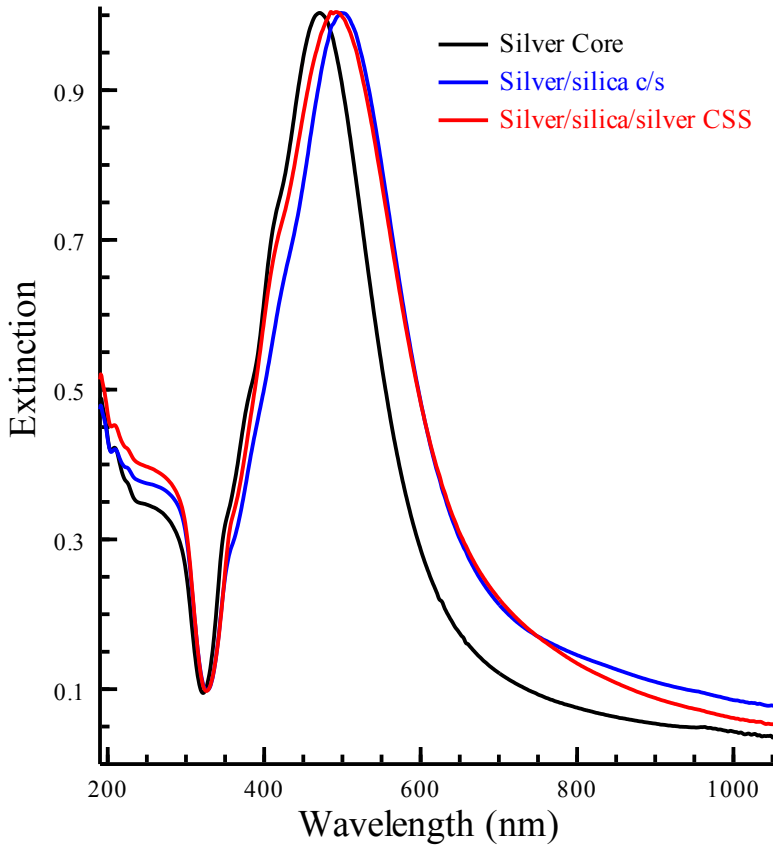

Figure 18. Extinction spectra of each step of the CSS particle synthesis.

A study was performed to confirm that the $[Ru(bpy)_3]^{2+}$was embedded into the silica layer and wasn't in silica particles that were formed outside the silver particles during the spacer layer synthesis. During the Ag/silica core/shell synthesis a small percentage of the TMOS goes

towards synthesizing silica nanoparticles in solution. In order to confirm that the dye was getting into the silver/silica core/shell particles and not free silica particles, dye-labeled silica particles and dye-labeled silver/silica with the same concentration of $[Ru(bpy)_3]^{2+}$ and the same concentration of nanoparticles were analyzed with Raman spectroscopy. The Raman spectra were then compared to determine the enhancement of the $[Ru(bpy)_3]^{2+}$ emission caused by the addition of a silver core. As can be seen in Figure 19, the dye-labeled silica didn't produce a Raman signal while the dye-labeled silver/silica particles produced a strong signal. This indicates that the $[Ru(bpy)_3]^{2+}$ is in close enough proximity to the silver particle to experience the electromagnetic mode of Raman enhancement, which occurs because the electric field of the silver particle's plasmon resonance overlaps with the $[Ru(bpy)_3]^{2+}$ in the spacer layer and enhances the Raman scattering of the $[Ru(bpy)_3]^{2+}$ complex.

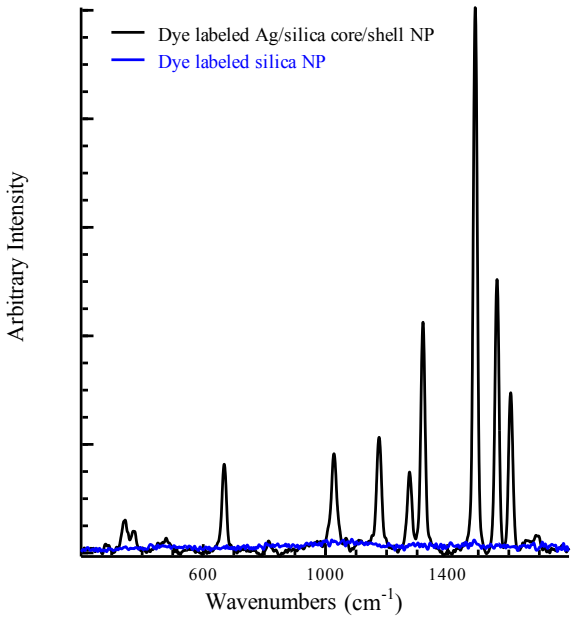

Figure 19. Raman spectra of the dye-labeled silica particles and the dye-labeled silver/silica core/shell particles. Both dye label concentrations and overall particle concentration were equivalent for each measurement.

After the dye-labeled particles were synthesized it was important to determine if there was an even distribution of $[Ru(bpy)_3]^{2+}$ in the particles. A study was completed in which the particle concentration of dye-labeled silver/silica was decreased in increments and the area of the 1490.1 cm^{-1} band of the SERS spectrum was calculated. The peak area was then plotted against the particle concentration (Figure 20). The linear fit (R^2=0.998) in Figure 20 shows that there is even distribution of $[Ru(bpy)_3]^{2+}$ throughout the CSS particles. Using beam waist and probe height measurements, the Raman scattering measurement volume was determined to be 35 pL. Using the results in Figure 20 and the probe volume it was determined that there are 420 ± 50 units of Raman intensity/particle at the 1490.1 cm^{-1} band. It was also approximated, using the probe volume and the concentration of $[Ru(bpy)_3]^{2+}$ per nanoparticle (Table 4), that the lowest particle concentration in Figure 20 (optical density 0.3) resulted in a concentration of $[Ru(bpy)_3]^{2+}$ of only 60 nM. According to previous studies in our lab, this concentration is at least two orders of magnitude lower than what can be detected with resonance Raman spectroscopy.[17]

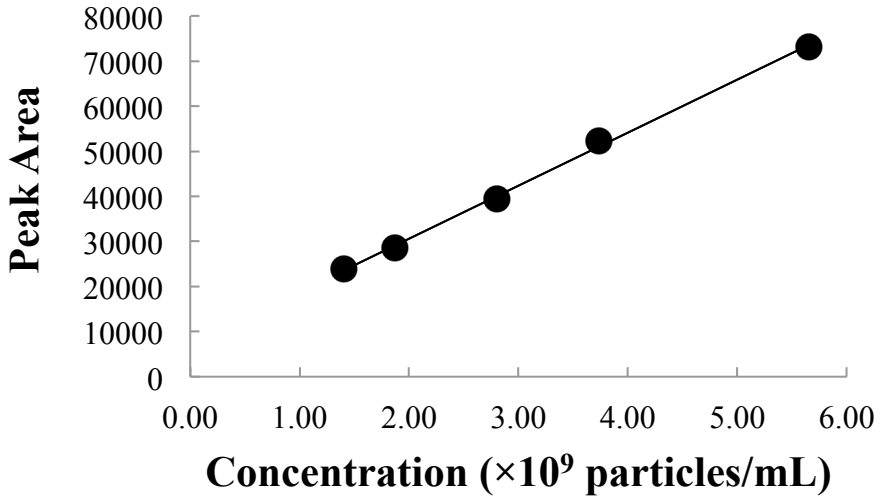

Figure 20. The peak area of the 1490.1 cm^{-1} peak of the Raman spectra vs. the particle concentration. The linear fit shows that there is an even distribution of $[Ru(bpy)_3]^{2+}$molecules in the particles.

After confirmation that the $[Ru(bpy)_3]^{2+}$was being embedded into the spacer layer of the particles, shells were grown onto the particles using the hydrogen reduction method after seeding the silica surface with the tin treatment followed by the silver (I) oxide soak and the synthesis was allowed to continue for three hours, which in previous research, was the typical time used for growing a complete shell.[17] It was found that after three hours the $[Ru(bpy)_3]^{2+}$Raman signal was no longer detectable so, presumably the shell was too thick. A study was completed to determine the maximum thickness of the shell for which a $[Ru(bpy)_3]^{2+}$ signal was still detectable. Aliquots were collected every five minutes during the hydrogen reduction synthesis of shells onto dye-labeled silver/silica core/shell particles over the course of 2.5 hours. The aliquots were then analyzed using Raman spectroscopy and the $[Ru(bpy)_3]^{2+}$ signal disappeared for particles that had reacted for only 30 minutes. The data is presented in Figure 21, and the spectra have been offset so the peak heights are more visible. Using the probe volume it was determined that there are only 288 particles in the collection volume. These spectra were collected with a 457.9 nm laser with a power of 10.3 mW at the sample and a 1 second collection time.

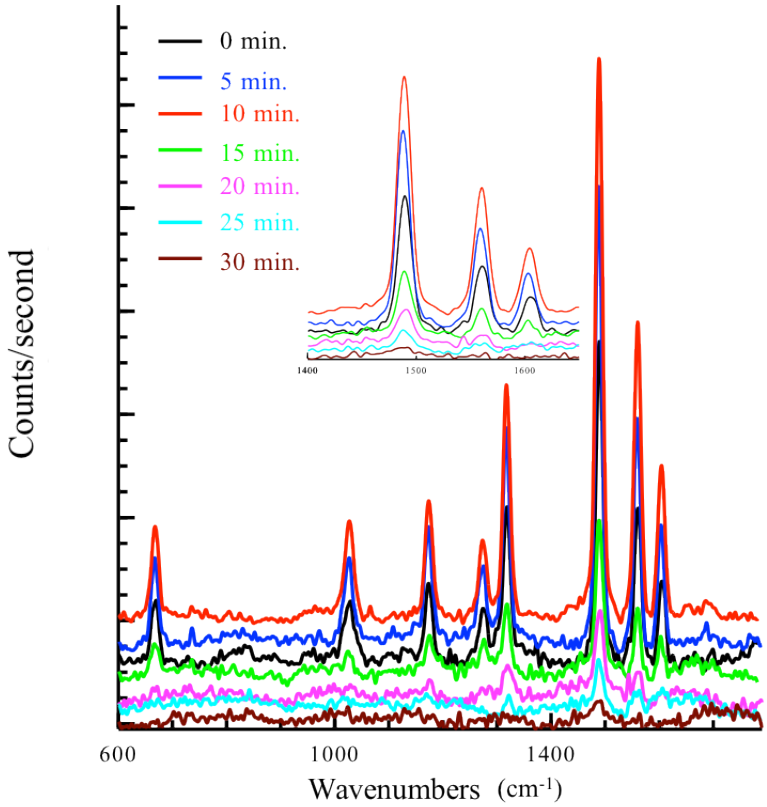

Figure 21. Raman spectra of the first seven aliquots collected during shell synthesis. After 30 minutes the $[Ru(bpy)_3]^{2+}$ signal is undetectable.

The first seven aliquots were then analyzed using the fluorometer (Figure 22) and the spectra reveals that as the silver is deposited onto the particle the fluorescence of the dye molecule in general decreases. This is contrary to what was expected because as silver is deposited onto the surface of the particle, a stronger coupling between the shell and core should occur, resulting in a stronger fluorescence signal. The only exception to this observation is for the 10 minute aliquot where the fluorescence intensity has increased relative to the 5 minute aliquot. It is interesting to note that in Figure 21 the highest Raman intensity peaks were also

obtained for the 10 minute aliquot. This suggests that there is some enhancement in the $[Ru(bpy)_3]^{2+}$ signal before the steady decrease.

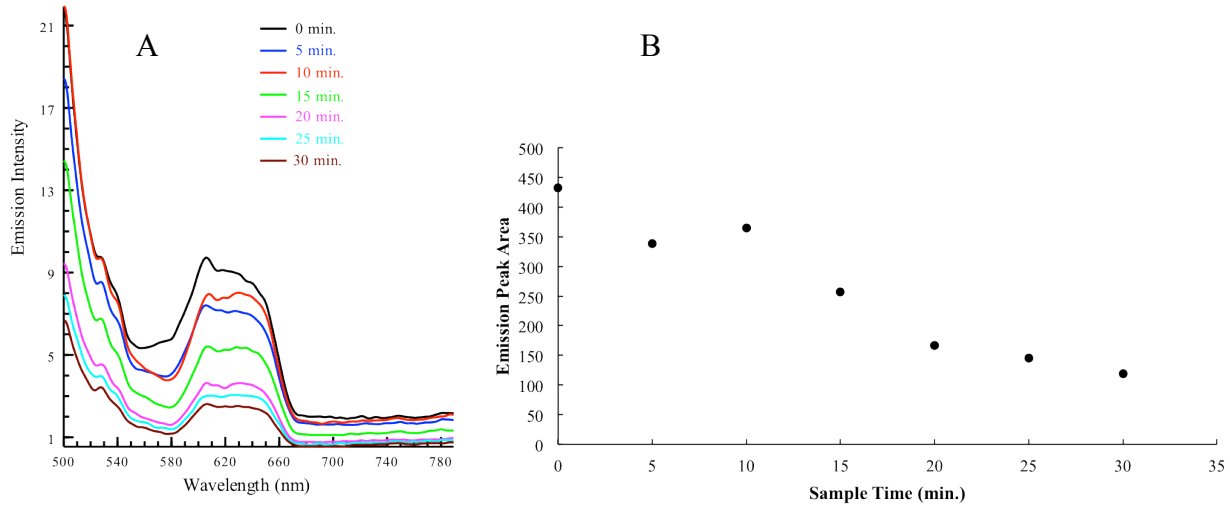

Figure 22. (A) Fluorescence spectra of five minute aliquots collected during the shell growth of CSS particles (B) Emission peak area plotted against the reaction time.

This fluorescence decrease was then explored more closely by measuring the extinction, absorption, and scattering of the particles and is presented in Figure 23. Figure 23 compares the silver/silica particles without a silver shell to CSS particles whose shell was synthesized for 30 minutes. As the shell is deposited onto the surface of the particle, the absorption component of the particle increases. This indicates that the silver shell is absorbing some of the source light. This may account for the decrease in fluorescence because the shell absorbs the source light, so less of the light is reaching the $[Ru(bpy)_3]^{2+}$ and so the fluorescence is decreasing. However, there are two other possibilities for the decrease in the fluorescence intensity. It is possible that the $[Ru(bpy)_3]^{2+}$ signal is being quenched because the silver shell is in direct contact or in close proximity to the dye. In order to achieve enhanced fluorescence, the dye molecule must be close enough to the metallic surface to experience both the electric field from the electron oscillations and near field scattering, but far enough away so the metallic surface doesn't quench the

$[Ru(bpy)_3]^{2+}$ emission. The final possibility is that the $[Ru(bpy)_3]^{2+}$ is emitting light but the light is being scattered. The collection volume for the fluorometer is narrow and even the slightest amount of scattering can make the signal undetectable.

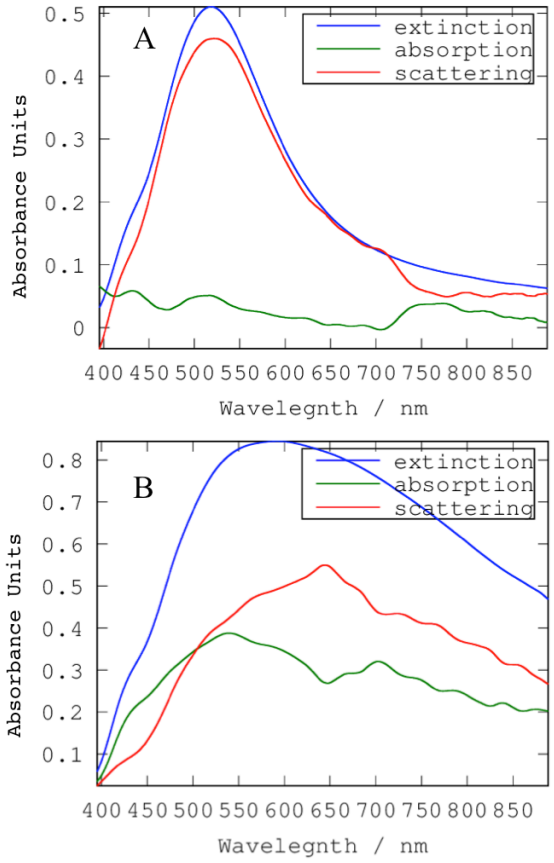

Figure 23. AES plots of (A) the dye-labeled silver/silica core/shell particles and (B) the dye-labeled silver/silica/silver CSS particles with a 30 minute shell synthesis.

The particle shells were found to have a higher absorption to scattering ratio than the silver/silica core/shell particles. As presented in Section 4.1.2The longer the plasmon lasts the longer the interaction between analyte molecules and the CSS particles. The increased interaction time results in better Raman enhancement of the analyte molecules. If a different dye molecule with a higher quantum yield than $[Ru(bpy)_3]^{2+}$ was utilized the shell absorption would still allow for a strong dye signal.

4.3.2 SILVER/SILICA/SILVER CSS PARTICLES WITH A 90 MINUTE SHELL SYNTHESIS

After the synthesis of particles with a 30 minute shell another set of particles were synthesized using a 90 minute shell synthesis. This was done because, as can be seen in Figure 17 (page 47), the thirty minute shell didn't result in a complete shell. By synthesizing particles with a 90 minute shell a more complete shell resulted (Figure 24). These particles were tested to determine their utility as an internal standard containing SERS substrate. Figure 24 also reveals that as time progresses the shell only slightly increases in diameter but the shell becomes more dense.

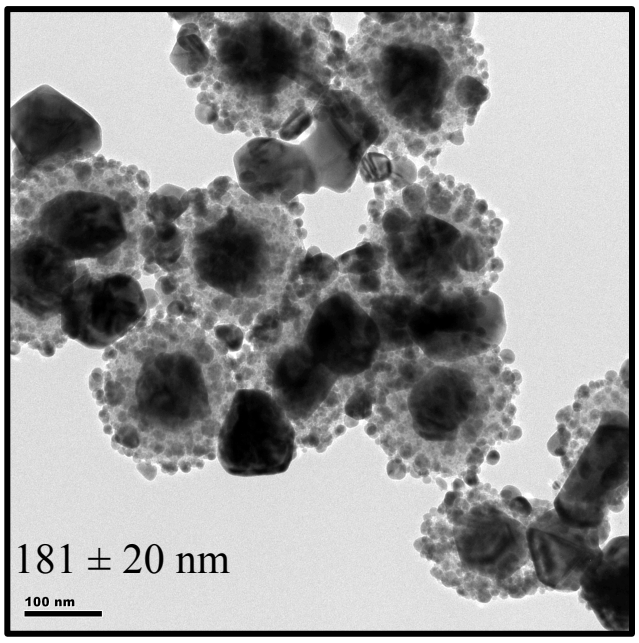

Figure 24. TEM image of CSS particles with a 90 minute hydrogen reduction shell synthesis.

The 90 minute shell particles were also analyzed using the integrating sphere to get the AES spectra of the particles. Comparison of the AES of the 90 minute shell with the 30 minute shell (Figure 25) shows that the absorption component of the extinction particles increases as the shell becomes more complete. This means that the 90 minute shell CSS particles would result in a better enhancement of an analyte signal during SERS.

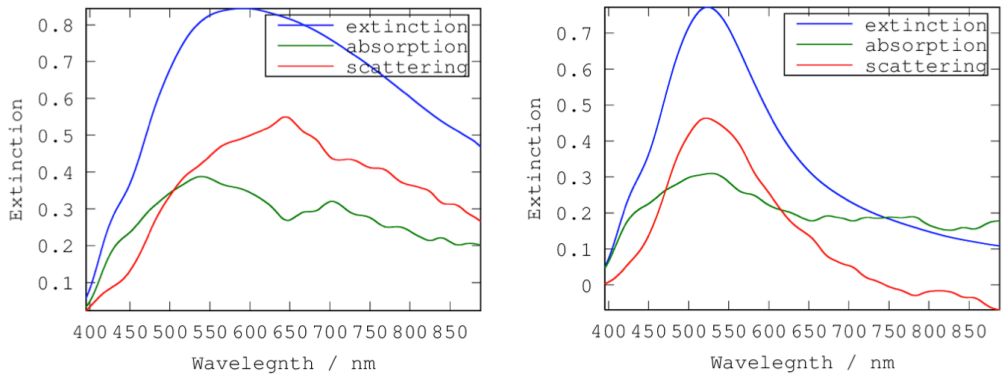

Figure 25. AES measurements of the CSS particles with (A) 30 minute shell, and (B) a 90 minute shell.

Finally, the 90 minute particles were used in a preliminary study to see if the dye-labeled particles can be used as an internal standard for SERS. In Figure 26 the $[Ru(bpy)_3]^{2+}$ dye was measured using the 457.9 nm laser and then a 1 μM solution of crystal violet (CV) that was mixed with the CSS particles was measured using the 632.8 nm laser line. Figure 26 shows that there are distinct bands that are measureable from both the $[Ru(bpy)_3]^{2+}$ (1490 cm^{-1}) and the crystal violet solution (800 and 900 cm^{-1}). The reason that a $[Ru(bpy)_3]^{2+}$ signal was detected for these 90 minute particles is because the particles were much more concentrated than in the previous section when the shell thickness was tested (Figure 21). It was calculated that there were 1.9×10^4 particles in the collection volume during this study compared to only 2.88×10^2 particles in Figure 21.

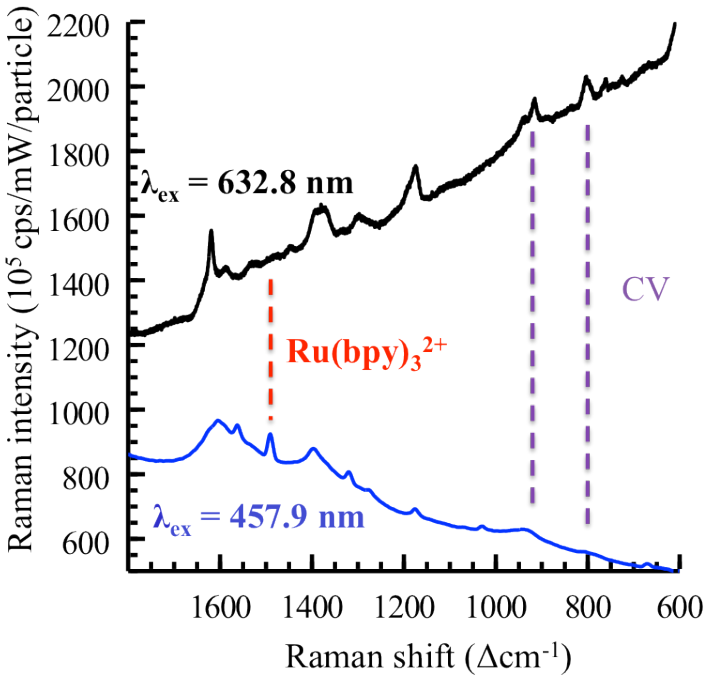

Figure 26. SERS spectrum of $[Ru(bpy)_3]^{2+}$ measured with a 457.9 nm laser (blue) and the spectrum of crystal violet measured with a 632.8 nm laser (black). There are unique $[Ru(bpy)_3]^{2+}$ peaks as well as crystal violet peaks in each of the spectra.

If another dye molecule is explored that has a higher quantum yield than $[Ru(bpy)_3]^{2+}$ a shell twice as thick as the 90 minute shell could be synthesized and a spectrum from the dye molecule could be obtained. This denser shell would allow for an even better analyte enhancement.

CHAPTER 5. CONCLUSIONS AND FUTURE WORK

The surface study has revealed that it is possible to synthesize silica/silver core/shell particles without adding any seed but by just functionalizing the surface of the particles with APTMS. The problem with this synthesis method is that the particles have a small absorption component and they mostly scatter light. A larger absorption component is important to increase the interaction between the silver and an analyte molecule. The best shells for Raman spectroscopy applications were synthesized using a tin treatment followed by a silver (I) oxide soak. The surface study also revealed that only doing a silver (I) oxide soak is undesirable because the surface of the particles undergoes a change that makes the particles difficult to centrifuge. However, if the silver (I) oxide soak could be slightly modified and a proper centrifuge process could be developed this would be desirable over the tin treatment and the silver (I) oxide soak because it would eliminate a complicated step.

This research provides evidence about the possibility to create core/spacer/shell particles with a dye molecule embedded into the spacer layer of the particle. Different shell thicknesses were explored during this study to find the maximum shell thickness that doesn't quench the Raman and fluorescence signal produced by $[Ru(bpy)_3]^{2+}$. It was determined that the shell absorbs a high amount of the excitation light and quickly quenches the $[Ru(bpy)_3]^{2+}$ due to the low quantum yield $[Ru(bpy)_3]^{2+}$. An even distribution of $[Ru(bpy)_3]^{2+}$ of molecules was found in each of the CSS particles with 29,000 dye molecules per nanoparticle. It was found that just by putting the dye molecule into the spacer layer near the silver core, the $[Ru(bpy)]_3^{2+}$ could be detected down to two orders of magnitude lower than what can be detected using RRS. The final experiment has shown the potential to use a dye-labeled CSS particle as an internal standard for SERS.

Future research will need to be done to look at the effect of the spacer layer on the signal produced by the dye molecule. In this research all of the spacer layers were approximately 50 nm in size which is generally considered a large spacer layer. If the spacer layer thickness is reduced there could be better coupling between the silver core and the outer silver shell. A different dye molecule is also going to be explored that has a higher quantum yield than $[Ru(bpy)_3]^{2+}$. The advantage of a dye molecule with a higher quantum yield is that a better fluorescence signal could be obtained because even though the silver shell would absorb some of the excitation light, the high quantum yield could overcome this slight absorption. The higher quantum yield would also allow for fluorescence lifetime measurements which were not able to be obtained for the $[Ru(bpy)_3]^{2+}$ dye-labeled CSS particles.

CHAPTER 6. WORKS CITED

(1) Kobayashi, Y.; Katakami, H.; Mine, E.; Nagao, D.; Konno, M.; Liz-Marzán, L. M. Silica Coating of Silver Nanoparticles Using a Modified Stober Method. *J. Colloid Interface Sci.* **2005**, *283*, 392–396.

(2) Rycenga, M.; Cobley, C. M.; Zeng, J.; Li, W.; Moran, C. H.; Zhang, Q.; Qin, D.; Xia, Y. Controlling the Synthesis and Assembly of Silver Nanostructures for Plasmonic Applications. *Chem. Rev.* **2011**, *111*, 3669–3712.

(3) Evanoff, D. D.; Chumanov, G. Synthesis and Optical Properties of Silver Nanoparticles and Arrays. *ChemPhysChem* **2005**, *6*, 1221–1231.

(4) Tejamaya, M.; Römer, I.; Merrifield, R. C.; Lead, J. R. Stability of Citrate, PVP, and PEG Coated Silver Nanoparticles in Ecotoxicology Media. *Environ. Sci. Technol.* **2012**, *46*, 7011–7017.

(5) Stöber, W.; Fink, A.; Bohn, E. Controlled Growth of Monodisperse Silica Spheres in the Micron Size Range. *J. Colloid Interface Sci.* **1968**, *26*, 62–69.

(6) Wright, J.; Sommerdijk, N. *Sol-Gel Materials Chemistry and Applications*; CRC Press: Boca Raton, **2001**.

(7) Albrecht, M.; Creighton, A.; Blatchford, C. Plasma Resonance Enhancement of Raman Scattering by Pyridine Adsorbed on Silver or Gold Sol Particles of Size Comparable to the Excitation Wavelength. *J. Chem. Soc., Faraday Trans. 2* **1979**, *75*, 790–798.

(8) Evanoff, D. D.; Chumanov, G. Size-Controlled Synthesis of Nanoparticles. 1. "Silver-Only" Aqueous Suspensions via Hydrogen Reduction. *J. Phys. Chem. B* **2004**, *108*, 13948–13956.

(9) Kalele, S.; Gosavi, S. W.; Urban, J.; Kulkarni, S. K. Nanoshell Particles : Synthesis , Properties and Applications. *Curr. Sci.* **2006**, *91*, 1038–1052.

(10) Flores, J. C.; Torres, V.; Popa, M.; Crespo, D.; Calderón-Moreno, J. M. Preparation of Core–shell Nanospheres of Silica–silver: SiO_2@Ag. *J. Non. Cryst. Solids* **2008**, *354*, 5435–5439.

(11) Jackson, J. B.; Halas, N. J. Silver Nanoshells: Variations in Morphologies and Optical Properties. *J. Phys. Chem. B* **2001**, *105*, 2743–2746.

(12) Westcott, S. L.; Oldenburg, S. J.; Lee, T. R.; Halas, N. J. Formation and Adsorption of Clusters of Gold Nanoparticles onto Functionalized Silica Nanoparticle Surfaces. *Langmuir* **1998**, *7463*, 5396–5401.

(13) Lu, L.; Sun, G.; Xi, S.; Wang, H.; Zhang, H.; Wang, T.; Zhou, X. A Colloidal Templating Method To Hollow Bimetallic Nanostructures. *Langmuir* **2003**, *19*, 3074–3077.

(14) Brito-Silva, A. M.; Sobral-Filho, R. G.; Barbosa-Silva, R.; de Araújo, C. B.; Galembeck, A.; Brolo, A. G. Improved Synthesis of Gold and Silver Nanoshells. *Langmuir* **2013**, *29*, 4366–4372.

(15) Takeda, Y.; Komori, Y.; Yoshitake, H. Direct Stöber Synthesis of Monodisperse Silica Particles Functionalized with Mercapto-, Vinyl- and Aminopropylsilanes in Alcohol–water Mixed Solvents. *Colloids Surf., A.* **2013**, *422*, 68–74.

(16) Zhu, M.; Qian, G.; Hong, Z.; Wang, Z.; Fan, X.; Wang, M. Preparation and Characterization of Silica–silver Core-Shell Structural Submicrometer Spheres. *J. Phys. Chem. Solids* **2005**, *66*, 748–752.

(17) Cook, J. Synthesis of Ag:SiO2:Ag Core:Spacer:Shell Nanoparticles via the Hydrogen Reduction Method and the Characterization of Their Optical Properties, Western Carolina University, Cullowhee, **2014**.

(18) Hardikar, V.; Matijević, E.; Coating of Nanosize Silver Particles with Silica. *J. Colloid Interface Sci.* **2000**, 221, 133-136

(19) Evanoff, D. D.; White, R. L.; Chumanov, G. Measuring the Distance Dependence of the Local Electromagnetic Field from Silver Nanoparticles. *J. Phys. Chem. B* **2004**, *108*, 1522–1524.

(20) Zhang, J.; Gryczynski, I.; Gryczynski, Z.; Lakowicz, J. R. Dye-Labeled Silver Nanoshell−Bright Particle. *J. Phys. Chem. B* **2006**, *110*, 8986–8991.

(21) Zhang, P.; Guo, Y. Surface-Enhanced Raman Scattering inside Metal Nanoshells. *J. Am. Chem. Soc.* **2009**, *131*, 3808–3809.

(22) Zhang, J.; Fu, Y.; Lakowicz, J. R. Emission Behavior of Fluorescently Labeled Silver Nanoshell: Enhanced Self-Quenching by Metal Nanostructure. *J. Phys. Chem. C. Nanomater. Interfaces* **2007**, *111*, 1955–1961.

(23) Skoog, D. A.; Holler, F. J.; Crouch, S. R. *Principles of Instrumental Analysis.*; Thomson Brooks/Cole: Belmont, **2007**.

(24) Smith, E.; Dent, G. *Modern Raman Spectroscopy: A Practical Approach*; John Wiley & Sons: West Sussex, **2005**.

(25) Ball, D. *Physical Chemistry*; Second Ed.; Cengage Learning: Stamford, **2015**.

(26) Chalmers, J.; Griffiths, P. *Handbook of Vibrational Spectroscopy*; J. Wiley: New York, **2002**.

(27) Ferraro, J.; Nakamoto, K.; Brown, C. *Introductory Raman Spectroscopy*; Second Ed.; Academic Press: Amsterdam; London, **2003**.

(28) Aroca, R. *Surface-Enhanced Vibrational Spectroscopy*; John Wiley & Sons: West Sussex, **2006**.

(29) MacLaughlin, C. M.; Mullaithilaga, N.; Yang, G.; Ip, S. Y.; Wang, C.; Walker, G. C. Surface-Enhanced Raman Scattering Dye-Labeled Au Nanoparticles for Triplexed Detection of Leukemia and Lymphoma Cells and SERS Flow Cytometry. *Langmuir* **2013**, *29*, 1908–1919.

(30) Halvorson, R. a; Vikesland, P. J. Surface-Enhanced Raman Spectroscopy (SERS) for Environmental Analyses. *Environ. Sci. Technol.* **2010**, *44*, 7749–7755.

(31) Silverstein, D. W.; Milojevich, C. B.; Camden, J. P.; Jensen, L. Investigation of Linear and Nonlinear Raman Scattering for Isotopologues of $Ru(bpy)_3^{2+}$. *J. Phys. Chem. C* **2013**, *117*, 20855–20866.

(32) Gryczynski, I.; Malicka, J.; Holder, E.; DiCesare, N.; Lakowicz, J. R. Effects of Metallic Silver Particles on the Emission Properties of $[Ru(bpy)_3]^{2+}$. *Chem. Phys. Lett.* **2003**, *372*, 409–414.

(33) Liu, T.; Li, D.; Yang, D.; Jiang, M. An Improved Seed-Mediated Growth Method to Coat Complete Silver Shells onto Silica Spheres for Surface-Enhanced Raman Scattering. *Colloids Surf., A.* **2011**, *387*, 17–22.

(34) Evanoff, D. D.; Chumanov, G. Size-Controlled Synthesis of Nanoparticles. 2. Measurement of Extinction, Scattering, and Absorption Cross Sections. *J. Phys. Chem. B* **2004**, *108*, 13957–13962.